Formation, radiative forcing, and climatic effects of severe regional haze

Yun Lin[1,2*], Yuan Wang[3*], Bowen Pan[1,4], Jiaxi Hu[1,5], Song Guo[6], Misti Levy Zamora[1,7], Pengfei Tian[1,8], Qiong Su[9], Yuemeng Ji[1,10], Jiayun Zhao[11], Mario Gomez-Hernandez[11], Min Hu[6], Renyi Zhang[1,11*]

[1]Department of Atmospheric Sciences, Texas A&M University, College Station, TX 77843, USA
[2]Joint Institute for Regional Earth System Science and Engineering (JIFRESSE), University of California at Los Angeles, Los Angeles, CA 90064
[3]Division of Geological and Planetary Sciences, California Institute of Technology, Pasadena, CA 91125, USA
[4]Department of Atmospheric Science, Colorado State University, Fort Collins, CO, 80521, USA
[5]Cooperative Institute for Mesoscale Meteorological Studies, NOAA/OAR National Severe Storms Laboratory, Norman, OK, USA
[6]State Key Joint Laboratory of Environmental Simulation and Pollution Control, College of Environmental Sciences and Engineering, Peking University, Beijing, 10087, P.R. China
[7]Department of Public Health Sciences, School of Medicine, University of Connecticut, Farmington, CT USA, 06030-6325
[8]Key Laboratory for Semi-Arid Climate Change of the Ministry of Education, College of Atmospheric Sciences, Lanzhou University, Lanzhou 730000, P. R. China
[9]Water Management & Hydrological Science, Texas A&M University, College Station, TX 77843, USA
[10]Guangzhou Key Laboratory of Environmental Catalysis and Pollution Control, School of Environmental Science and Engineering, Institute of Environmental Health and Pollution Control, Guangdong University of Technology, Guangzhou 510006, China
[11]Department of Chemistry, Texas A&M University, College Station, TX 77843, USA

*Correspondence: yunlin@ucla.edu; Yuan.Wang@caltech.edu; renyi-zhang@tamu.edu

Abstract. Severe regional haze events, which are characterized by exceedingly high levels of fine particulate matter (PM), occur frequently in many developing countries (such as China and India), with profound implications for human health, weather, and climate. The occurrence of the haze extremes involves a complex interplay between primary emissions, secondary formation, and conducive meteorological conditions, and the relative contributions of the various processes remains unclear. Here we investigated severe regional haze episodes in 2013 over the Northern China Plain (NCP), by evaluating the PM production and the interactions between elevated PM and the planetary boundary layer (PBL). Analysis of the ground-based measurements and satellite observations of PM properties shows nearly synchronized temporal PM variations among the three megacities (Beijing, Baoding, and Shijiazhuang) in this region and a coincidence of the aerosol optical depth (AOD) hotspots with the three megacities during the polluted period. During the clean-to-hazy transition, the measured oxygenated organic aerosol concentration ([OOA]) well correlates with the odd-oxygen concentration ($[O_x] = [O_3] + [NO_2]$), and the mean $[OOA]/[O_x]$ ratio in Beijing is much larger than those in other megacities (such as Mexico City and Houston), indicating highly efficient photochemical activity. Simulations using the Weather Research and Forecasting (WRF) model coupled with an explicit aerosol radiative module reveal that strong aerosol-PBL interaction during the polluted period results in a suppressed and stabilized PBL and elevated humidity, triggering a positive feedback to amplify the haze severity at the ground level. Model sensitivity study illustrates the importance of black carbon (BC) in the haze-PBL interaction and the aerosol regional climatic effect, contributing to more than 30% of the PBL collapse and about half of the positive radiative forcing on the top of the atmosphere. Overall, severe regional haze exhibits strong negative radiative forcing (cooling) of -63 to -88 W m^{-2} at the surface and strong positive radiative forcing (warming) of 57 to 82 W m^{-2} in the atmosphere, with a slightly negative net radiative forcing of about -6 W m^{-2} on the top of the atmosphere. Our work

establishes a synthetic view for the dominant regional features during severe haze events, unraveling rapid *in-situ* PM production and inefficient transport, both of which are amplified by atmospheric stagnation. On the other hand, regional transport sufficiently disperses gaseous aerosol precursors (e.g., sulfur dioxide, nitrogen oxides, volatile organic compounds, and ammonia) during the clean period, which subsequently result in rapid *in-situ* PM production via photochemistry during the transition period and via multiphase chemistry during the polluted period. Our findings highlight the co-benefits for reduction in BC emissions, which not only improve local and regional air quality by minimizing air stagnation but also mitigate the global warming by alleviating the positive direct radiative forcing.

1. Introduction

Rapid economic growth and urbanization have caused frequent severe regional haze events associated with heavy pollution of particulate matter (PM) in many developing countries, including China and India (Bouarar et al., 2017; Molina, 2021). The severe haze events induce great degradation in visibility and air quality, with profound societal implications (An et al., 2019). For example, exposure to elevated levels of fine PM leads to adverse health effects, ranging from aggravated allergies to the development of chronic diseases, to premature death (Pope and Dockery, 2015; Wu et al., 2019; Rychlik et al., 2019; Johnson et al., 2021; Zhang et al., 2021). Also, elevated levels of fine aerosols result in pronounced modifications to clouds, precipitation, and lightning, impacting regional/global weather and climate (Zhang et al., 2007; Yuan et al., 2008; Qian et al., 2009; Wang et al., 2011; Wang et al., 2014; Wu et al., 2016). Specifically, by absorbing/scattering solar radiation, aerosols impact the atmospheric stability and the energy budget of Earth, via the aerosol-radiation interaction (ARI). By serving as cloud condensation nuclei (CCN) and ice nucleating particles (INPs), aerosols influence the macro- and microphysical properties of clouds, via the aerosol–cloud interaction (ACI). Currently, the radiative forcing associated with ARI and ACI represents the largest uncertainty in the projection of future climate by anthropogenic activities (IPCC, 2013).

PM is either emitted directly into the atmosphere (primary) or produced in air via gas-to-particle conversion (secondary) (Zhang et al., 2015a). Primary and secondary PM also undergo chemical and physical transformations and are subjected to cloud processing and removal from air (Zhang et al., 2015a). Direct emissions of primary gases and PM and highly efficient secondary PM formation represent the primary processes leading to severe haze (Guo et al., 2014; Sun et al., 2014; Wang et al., 2016a;). Haze evolution typically exhibits distinctive secondary aerosol formation, which is linked to several chemical and physical processes, that is, new particle formation and aerosol growth driven by photochemistry during the clean stage

and aqueous chemistry during the transition stage as well as the interaction between aerosols and atmospheric stability relevant to solar radiation absorption (Zhang et al., 2009; Xu and Zhang, 2012; Ji et al., 2020; Peng et al., 2021). In addition, conducive weather conditions for pollutant accumulation, such as regional control by high-pressure, suppressed local circulations, and weakened large-scale circulation, correspond to the external causes for severe haze formation (Liu et al., 2013; Wang et al., 2014d; Cai et al., 2017; Li et al., 2019).

The key constituents of fine PM include secondary inorganic (including sulfate, nitrate, and ammonium) aerosol (SIA) and secondary organic aerosol (SOA), with the corresponding gaseous precursors of sulfur dioxide (SO_2), nitrogen oxides (NO_x = NO + NO_2), ammonia (NH_3), and volatile organic compounds (VOCs). The photochemistry represents one of the mechanisms leading to SIA and SOA accumulation during the early stage of haze evolution (Guo et al., 2014; Zhang et al., 2015a; Wang et al., 2016; Zhang et al., 2020). Field measurements have shown that remarkably nucleation and growth of nanoparticles are primarily driven by photochemical activity, which is characterized by elevated ozone levels and efficient photolysis rate coefficients under clean daytime conditions (Zhang et al., 2015b; Guo et al., 2020). During haze evolution, the photochemical activity is typically reduced, as evident by low levels of ozone and reduced photolysis rates (Peng et al., 2021). On the other hand, there are increasing air stagnation and relative humidity (RH), when explosive secondary aerosol formation occurs (Peng et al., 2021). The latter has been attributed the occurrence of multiphase chemistry, which largely drives the formation of SIA and SOA during the polluted period (Peng et al., 2021). Currently, the relative contributions of primary emissions, secondary production, and regional transport to severe haze formation remain uncertain (Li et al., 2015; Zhang et al., 2015b; Peng et al., 2021). Moreover, the efficiency of photochemical PM production during regional haze events in NCP and its distinction among various megacities worldwide remain to be quantified (Molina, 2021).

While the importance of regional haze on climate has been recognized (Ramanathan et al., 2007; Wang et al., 2009; Wang et al., 2015a), there still lacks quantification for the aerosol radiative forcing and the climatic effects for severe regional haze events. Estimation of the aerosol radiative forcing during severe haze events exhibits a large variation (Li et al., 2007; Xia et al., 2007; Wang et al., 2009; Che et al., 2014). In addition, the interactions between aerosols and planetary boundary layer (PBL) via the aerosol radiative effects likely increase the haze severity (Wang et al., 2015a; Wang et al., 2016b; Zhang et al., 2018). Meteorological conditions within the PBL, including the atmospheric stability and RH, are altered by the aerosol-PBL interaction to induce a positive feedback to PM accumulation near the ground level (Tang et al., 2016a; Tie et al., 2017; Wu et al., 2020). However, the aerosol-PBL interactions and their feedbacks to atmospheric thermodynamics and dynamics under extremely hazy conditions remain to be quantified (Li et al., 2017).

Previous studies have documented the role of black carbon (BC) in the aerosol-PBL interactions and the aerosol regional climate effects (Menon et al., 2002; Bond et al., 2013; Wang et al., 2013; Ding et al., 2016). In addition, the BC aging process markedly enhances BC absorption by modifying the particle physiochemical and optical properties (Zhang et al., 2008; Khalizov et al., 2013; He et al., 2015; Guo et al., 2016; Peng et al., 2016; Peng et al., 2017). For example, an experimental/field study showed that the mass absorption cross section (MAC) of BC is enhanced by 2.4 times in a short time because of BC aging under polluted urban conditions (Peng et al., 2016), reconciling previous variable results on the coating-enhanced absorption for BC (Gustafsson and Ramanathan, 2016). Apparently, the enhancement of the BC absorption causes additional aerosol radiative forcing (Peng et al., 2016) and suppression on PBL development (Wang et al., 2017). Currently, limited modeling studies have assessed the radiative effect of BC aging associated with severe regional haze (Wang et al., 2013; He et al., 2015; Gustafsson and Ramanathan, 2016).

To better understand the formation and evolution of severe regional haze as well as their regional and climate effects, we investigated severe haze episodes occurring in 2013 over the Northern China Plain (NCP). The NCP region, which encompasses the megacities of Beijing and Tianjin, and some portion of the provinces of Heibei, Shandong, and Henan, represents the most polluted area in China (An et al., 2019). Satellite observations and field measurements of PM properties were evaluated, and numerical simulations were performed to elucidate the interactions between severe haze and PBL using Weather Research and Forecast (WRF) model coupled with an explicit aerosol radiative module (Fan et al., 2008; Wang et al., 2014c). By conducting model sensitivity simulations, we elucidated the impacts of BC aging on the haze-PBL interactions and its contribution to the net aerosol radiative forcing during severe haze periods.

2. Methodology

The NCP represents a key economic zone in China, as reflected by its gross domestic product (GDP), energy consumption, and vehicular fleets (An et al., 2019). The region has undergone fast industrialization and urbanization over the past four decades. For example, NCP is one of the most densely populated regions in the world and contributes to over 1/10 of the GDP in China. The consumption of coal and crude oil in NCP was 363 and 72 million tons, respectively, to 1,348 million tons in 1998 and increased to 140 million tons of standard coal equivalent in 2010, respectively. In particular, anthropogenic activities result in industrial, traffic, residential, and agricultural emissions, representing the major sources for PM precursors, including SO_2, NO_x, VOCs, and NH_3 (An et al., 2019; Peng et al., 2021). Surrounded by the Taihang Mountains to the west and Yanshan Mountains to the north, respectively, the NCP region is prone to develop air stagnation under conducive meteorological conditions, inhibiting vertical and horizontal dispersion of air pollutants (An et al., 2019; Peng et al., 2021).

2.1. The Data Sources

The satellite-retrieved aerosol optical depth (AOD) was derived by combining the Moderate Resolution Imaging Spectroradiometer (MODIS) measurements of Aqua and Terra using the equal-weighted mean method to increase the spatial coverage (Levy et al., 2009). The MODIS data are accessible at http://giovanni.gsfc.nasa.gov/aerostat/. The Terra visible images were obtained at https://worldview.earthdata.nasa.gov/. The hourly PBL height used was based on the Modern-Era Retrospective analysis for Research and Applications, Version 2 (MERRA2) reanalysis data. The severe haze days were selected with daily $PM_{2.5}$ (particular matter with aerodynamic diameter less than 2.5 micron) concentration greater than 200 μg m^{-3}, and the typical clean days were limited to the days with daily $PM_{2.5}$ concentration smaller than 30 μg m^{-3}. The PBL height and the $PM_{2.5}$ surface concentration at 14:00 Beijing time (BJT) each day in 2013 were used for the correlation analysis. All raining days were filtered out when analyzing the correlation between the PBL height and the $PM_{2.5}$ concentration. The surface solar radiation (SSR) data were based on the satellite retrievals (Tang et al., 2016b), which are accessible at http://www.tpedatabase.cn.

Ground-based measurements of fine particulate matter or $PM_{2.5}$ employed in our analysis covered the period from 25 September to 14 November 2013. The hourly $PM_{2.5}$ concentrations in Beijing (BJ) were obtained from the Embassy of United States in Beijing (http://www.stateair.net/web/historical/1/1.html). The $PM_{2.5}$ mass concentrations in Baoding (BD) and Shijiazhuang (SJZ) were obtained from https://air.cnemc.cn:18007/. Measurements of PM properties in Beijing were taken from that previously reported by Guo et al. (2014), which provided $PM_{2.5}$ concentration, aerosol chemical composition, and gaseous data for correlation analysis and constrains for modeling studies. For example, the mass concentrations of various inorganic and organic aerosol species, including oxygenated organic aerosol (OOA), were measured using an aerosol mass spectrometer (AMS) in Beijing (Aiken et al., 2009; Guo

et al., 2014). The observation-based analysis and the modeling study focused on two severe haze episodes, i.e., 25 September – 30 September (episode 1 or EP1) and 2 October – 6 October (episode 2 or EP2), 2013 in NCP.

2.2. Model experiments

2.2.1. Simulations on the haze-PBL interactions

The aerosol-PBL interactions during the severe haze events and the associated regional climate effects were examined by conducting WRF modeling sensitivity studies. An aerosol radiative module was implemented by Fan et al. (2008) to the Goddard Shortwave Radiation Scheme to online compute the wavelength-dependent aerosol optical properties, including the AOD, the asymmetry factor and the single scattering albedo (SSAs). Aerosol particles with the core-shell configuration in the aerosol radiative module were assumed to consist of BC (core) and ammonia sulfate (shell). The hygroscopic growth of aerosol particles was taken into account, following Mallet et al. (2004). A two-moment bulk microphysical scheme developed by Li et al. (2008) was employed, which has been widely used to investigate the aerosol-cloud interactions under various cloud systems (Wang et al., 2014b; Wang et al., 2014a; Lin et al., 2016). A 100×100 grids domain with a horizontal grid spacing of 2 km and 50 vertical levels with stretched grid spacings was set up to cover the entire urban region of Beijing. The initial and boundary meteorological conditions were generated from six-hourly NCEP FNL (Final) Operational Global Analysis (1°×1°). No convective parametrization was applied for the simulations.

We performed simulations on the two haze episodes (EP1 and EP2). The two days prior to the two haze episodes (25 September and 2 October, 2013) are denoted as the clean periods, while the most polluted days during the two episodes, i.e., 28 September and 5 October are denoted as the polluted periods. The aerosol number size distributions for initial and boundary conditions of all simulation were based on the measurements during the 2013 field campaign

at Beijing (Fig. S1). The aerosol measurements on 25 September and 2 October 2013 were taken as the input for the clean cases and 28 September and 5 October 2013 for the polluted cases. The aerosol surface number and mass concentration for modeling initialization were set as 3.5×10^4 cm^{-3} (3.6×10^4 cm^{-3}) and 10 μg m^{-3} (11 μg m^{-3}) for the clean case of EP1 (EP2) and 1.7×10^4 cm^{-3} (1.8×10^4 cm^{-3}) and 280 μg m^{-3} (310 μg m^{-3}) for the polluted case of EP1 (EP2), respectively, consistent with the field measurements. Also, based on the measurements, the BC percentage in total aerosol mass was set as 10.0% and 6.0% for the clean and polluted cases, respectively. The two polluted days for simulations were cloud-free days, therefore the aerosol indirect effects were ruled out.

To assess the role of BC in the aerosol suppression effect on the PBL development and the aerosol radiative forcing during haze evolution, we performed a set of sensitivity simulations under the polluted condition by excluding the BC effects (referred as non-BC case), in which the BC radiative effect was turned off by assigning a zero value to the real and imaginary parts of BC refractive index, i.e., the SSA in non-BC case was equal to unity. To quantify the BC aging effects, additional simulations were carried out for fresh BC (denoted by fresh-BC), in which the BC core was not imbedded in the non-BC shell and the optical parameters for the BC and non-BC components were calculated separately by the Mie theory. In the fresh-BC case, the lensing effect due to the coating during the aging process was excluded, but the restructuring effect induced by aging was considered partially since the BC core was assumed to be spherical and in the compact shape. Alternatively, a case for aged BC (denoted by aged-BC) was treated by considering the full aerosol components (with both BC and non-BC components) and the core-shell configuration. A summary of the simulation cases is listed in Table 1.

One deficiency to predict the absorbed AOD and the directive radiation forcing of BC in atmospheric models is relevant to the underestimation in coating-enhancement of BC

absorption (Bond et al., 2013). To assess the potential bias on the radiative effects of aged BC, additional simulations on the polluted conditions were conducted by constraining the enhancement of mass absorption cross section of BC ($E_{MAC\text{-}BC}$) according to the experimental value, i.e., 2.4, derived from a chamber study in Beijing (Peng et al., 2016). Though the $E_{MAC\text{-}BC}$ of 2.3 derived from the aged-BC case is slightly lower than that reported by Peng et al. (2016), comparison between the two simulations indicates little difference in the thermodynamic/dynamic conditions and the radiative budget.

2.2.2. Empirical estimation of the moisture effect on haze-PBL interactions

In addition to the numerical model simulations, we employed an empirical equation derived by Nozaki (1973) and modified by Tie et al. (2017) to examine the RH sensitivity in the boundary layer to the PBL height based on observed meteorological conditions:

$$H = \frac{121}{6}(6 - P)(T - T_d) + \frac{0.169P(U_Z+0.257)}{12f \ln Z/z_0} \quad (1)$$

where H, T, T_d, and U_z represent the PBL height (m), surface air temperature (K), surface dew point (K), and mean wind speed (m s^{-1}) at height of Z (Z=10 m), respectively. f and z_0 are the Coriolis parameter (s^{-1}) and surface roughness length (0.5 m in this study), respectively. P is the Pasquill stability level, classified as six categories from very unstable (A), moderately unstable (B), slightly unstable (C), neutral (D), slightly stable (E) to moderately stable (F) (Pasquill, 1961). To relate RH with the PBL height, we adopted a modified Nozaki's equation using (100- RH)/5 to replace (T-T_d) according to Wallace and Hobbs (2005) and Tie et al. (2017). The measured wind speeds were used in the calculations. For the severe haze events, the atmosphere was stable, and the Pasquill stability levels were set as 4~5. The inputs of the PBL height for the clean and aged-BC cases were based on ceilometer measurements, showing that the PBL height increased by about 700~900 m from the aged-BC to the clean cases.

3. Results and Discussion

3.1. Regional characteristics of severe haze episodes

Measurements of the $PM_{2.5}$ mass concentrations from 25 September to 14 November 2013 reveal that severe haze occurs frequently over the NCP, reflected by a periodic cycle of 4-7 days with highly elevated PM pollution (Fig. 1a-c). Each severe haze episode consists of a clean period, a transition period from clean to hazy conditions, and a polluted period with very high PM levels. For the three megacities across the NCP, i.e., Beijing, Baoding, and Shijiazhuang, the maximal mass concentration of $PM_{2.5}$ consistently exceed several hundred μg m^{-3} during the polluted period. The $PM_{2.5}$ concentrations at the three megacities exhibit a remarkable similarity in the timing and magnitude for the peak $PM_{2.5}$ concentrations. The nearly synchronized temporal variations in the PM levels among the three megacities indicate a prominent characteristic of severe haze formation, indicating the importance of *in-situ* PM production over the entire region. During the evolution from clean, transition, to polluted periods, the RH and wind speed is consistently increased and decreased, respectively (Fig. 1d).

The two polluted events on 28 September (EP1) and 5 October (EP2) are captured from both *in-situ* measurements (Fig. 1) and satellite observations (Fig. 2). The satellite MODIS data illustrate that the maximal AOD area occurs in the three megacities (i.e., BJ, BD, and SJZ). For example, the AOD value in Beijing exceeds 4.0 and 2.0, during EP1 and EP2, respectively. The spatial distribution of severe regional haze events is also depicted from the satellite visible images, showing that a grey haze plume covers a substantial portion of the NCP region (Figs. 2c and d). The coincidence of the highest AOD areas with the locations of the megacities is also discernable from the mean AOD values averaged over all the hazy days (e.g., daily $PM_{2.5}$ > 200 μg m^{-3}) in 2013 (Fig. S3), showing a large zone of elevated AOD values over the three megacities. In contrast, the fall seasonal and annual AOD means averaged over all days in 2013 show that the maximal AOD values are located to the south of Beijing (Figs. 2e and f),

reflecting the typical regional transport pattens over this region (Guo et al., 2014; An et al.,2019; Peng et al., 2021). In addition, the occurrence of severe haze events is consistently accompanied by stagnant weather, characterized by weak southerly winds in Beijing and its surrounding areas (Figs. 2a and b). For example, the wind speed is typically less than 1 m s^{-1} in the highest AOD area (Figs. 2a and b), compared to that of a few to ten m s^{-1} during the clean period (Fig. 1d). Air stagnation retards PM dispersion, resulting in minimal regional transport during the polluted period. On the other hand, the gaseous aerosol precursors (e.g., SO_2, NO_x, VOCs, and NH_3 with the chemical lifetimes from hours to days) are sufficiently transported and dispersed prior to haze development over this region, as evident from much higher wind speeds during the clean period (Fig. 1d). Efficient regional transport of the gaseous aerosol precursors explains the similarity in the spatial/temporal PM variations, since well-mixed gaseous aerosol precursors result in similar *in-situ* PM production under stagnant conditions (Figs. 1a-c). Moreover, the coincidence of the AOD hotspots with the three megacities (Figs. 2a, b and S3) indicates more efficient *in-situ* PM production over the megacities, suggesting a key role of traffic emissions (i.e., anthropogenic VOCs and NO_x) in facilitating regional severe haze formation. While wind fluctuation likely results in PM variation in an isolated location, especially for Beijing, which is situated at the northern edge of the NCP (Li et al., 2015), our analysis of temporal/spatial PM distributions indicates that the dominant regional features during the polluted period are reflected by rapid *in-situ* PM production and inefficient transport, both of which are amplified by air stabilization.

3.2. Photochemical PM formation

To further elucidate the role of *in-situ* photochemical production in haze development, we analyzed the temporally resolved PM properties in Beijing. Typically, haze evolution in this region involves new particle formation and subsequently growth of nucleation mode particles during the clean period, which are mainly driven by photochemistry (Lee et al., 2019;

315 Guo et al., 2020). Evidently, the $PM_{2.5}$ mass concentration increases by more than 200 μg m^{-3}
316 in less than 8 hrs. during the transition period for EP1 and EP2 (Figs. 3a and b), which is
317 dominated by the increase in the SOA mass concentration linked to photochemical oxidation
318 of VOCs (Guo et al., 2014; Liu et al., 2021). The mass concentration of OOA is typically
319 considered as a surrogate for SOA (Wood et al., 2010). Since OOA and the level of oxidants,
320 O_x ($[O_x] \equiv [O_3] + [NO_2]$), are both produced from oxidation of VOCs (Suh et al., 2001; Fan
321 and Zhang, 2004; Zhao et al., 2004, 2005; Ji et al., 2017) and have a lifetime of longer than 12
322 hours, it is anticipated that both quantities are correlated, when their formations occur on a
323 similar timescale and at the same location (Atkinson, 2000). Figs. 3a-d show that the increase
324 in OOA is well correlated with the O_x level during the transition period. The R^2 from linear
325 regression between OOA and O_x during the transition period (i.e., from 7:00 am to 2:30 pm) is
326 0.96 for EP1 and 0.95 for EP2 (Fig. 3e). The high correlation between OOA and O_x implies
327 important *in-situ* production of PM via photochemical reactions, consistent with the ground-
328 based measurements (Fig. 1) and satellite observations for PM (Fig. 2 and Fig. S3). The mean
329 ratio of [OOA] to [O_x] for the two episodes in Beijing is 0.34 (μg m^{-3} ppb^{-1}), suggesting highly
330 efficient photochemistry. For comparison, the mean ratio of [OOA] to [O_x] during the two
331 episodes in Beijing is about 2.4 and 5.1 times of those in Mexico City and Houston (Wood et
332 al., 2010), respectively, indicating that the photochemical PM formation in Beijing is much
333 more efficient than those in Mexico City and Houston (Fig. 3f). The more efficient
334 photochemical formation of PM in Beijing is attributable to the presence of higher levels of
335 anthropogenic aerosol precursors, such as anthropogenic VOCs and NO_x, than those in the
336 other two cities (Guo et al., 2014; Zhang et al., 2015a). On the other hand, the correlation
337 between [OOA] and [O_x] exists only during the transition stage but vanishes during the polluted
338 period. The latter is evident from the continuing increase in [OOA] but decreasing [O_x]. In
339 particular, O_3 production is significantly suppressed during the polluted periods because of

reduced solar ultraviolet radiation, leading to inefficient photooxidation (Wu et al., 2020; Peng et al., 2021). Several previous studies have attributed highly elevated levels of $PM_{2.5}$ during the polluted period to the importance of multiphase chemistry to contribute to SIA and SOA formation (Wang et al., 2016; An et al., 2019; Peng et al., 2021). For example, sulfate formation is effectively catalyzed by BC (Zhang et al., 2020) and considerably enhanced via aqueous oxidation of SO_2 by NO_2 in the presence of NH_3 during the transition/polluted periods (Wang et al., 2016), both increasing with increasing RH. Also, oligomerization from dicarbonyls increases at high RH (Li et al., 2021a, b), contributing to significantly enhanced SOA formation during the polluted periods (Zhang et al., 2021).

Note that both the photochemical production and PBL evolution contribute to PM accumulation at the ground level, since the PBL development leads to vertical ventilation and dilution during the daytime. The ceilometer-retrieved PBL height increases about 200 m (150 m) from morning to afternoon and decreases by about 150 m (400 m) from afternoon to midnight on 27 September (4 October) (Fig. S4). Clearly, the largest PM increase as well as the strong correlation between OOA and O_x during the morning and early afternoon hours indicate that the photochemical production dominates the PM increase during the transition period.

3.3. Impacts of the haze-PBL interaction

3.3.1. A positive feedback of PM accumulation

To assess the impacts of haze-PBL interactions on PM pollution, we evaluated the correlation between the PM level and PBL height. Fig. 4 shows an analysis of daily PBL height versus $PM_{2.5}$ concentration between clean and hazy days from the ground-based measurements and the MERRA2 reanalysis data in 2013. The daily PBL height is negatively correlated with surface $PM_{2.5}$ concentration (Fig. 4a). The diurnal cycle of the PBL height shows that the PBL height on severe haze days (daily $PM_{2.5}$ concentration > 200 μg m^{-3}) is significantly lower than

365 that on clean days (daily $PM_{2.5}$ concentration < 30 μg m^{-3}), with a maximum difference of 800
366 m (Fig. 4b). Furthermore, the dimming area over NCP, which is reflected by the lower mean
367 of the satellite-retrieved surface solar radiation (SSR) averaged over all the severe haze days
368 in 2013, coincides with the region with the highest AOD (Fig. S3), implying a strong spatial
369 association between the solar radiation intensity and PM pollution at the surface. The co-
370 locations in the areas between the lowest SSR and highest AOD also reflects the occurrence of
371 the highest PM levels at the megacities during the regional severe haze episodes.

372 We further elucidated the response of PBL development to the PM pollution, and the
373 linkage between the aerosol-PBL interactions and aerosol radiative effects are further
374 elucidated by performing sensitivity modeling studies on the two hazy days (Figs. 5-6). The
375 performance of the model simulations was validated by comparison with field observations.
376 The simulated temperature and RH are consistent with the sounding data in light of the vertical
377 variations (Fig. S2). The simulated AOD at 550 nm is 0.05 and 3.6 on 25 and 28 September
378 2013 for EP1, respectively, and 0.04 and 2.0 on 2 and 5 October 2013 for EP2, respectively, in
379 qualitative agreement with the Aerosol Robotic Network (AERONET) measurements in
380 Beijing (Table 2). The simulated one-day accumulated surface solar radiation and the peak
381 solar radiation flux in the aged-BC case for EP1 (EP2) are 9.2 MJ m^{-2} (11.3 MJ m^{-2}) and 326
382 W m^{-2} (402 W m^{-2}), respectively, comparable to the ground-based measurement of 10.6 MJ m^{-2}
383 (9.8 MJ m^{-2}) and 408 W m^{-2} (452 W m^{-2}) in Table 2. The temporal evolutions of PBL and its
384 peak heights derived from the aged-BC cases are also consistent with the available
385 measurements (Figs. 5a and g).

386 The simulated maximal height of PBL under the polluted condition is reduced by more
387 than 300 m relative to the clean condition (Figs. 5a and g). The reduction in PBL height is
388 explained by the aerosol radiative effects. Under the polluted condition, a warmer temperature
389 is located at the altitude of around 1.2 km, and less SSR reaches the ground level (Figs. 5e and

k, f and l). Also, the surface temperature is reduced by several degrees (Figs. 5e and k, and Figs. 6a and c). The extents of warming in the upper boundary layer and cooling at the surface due to the aerosol effect in this study are consistent with the observational analysis on North China by Huang et al. (2018), indicating that our simulations well reproduce the aerosol radiative effect under severe regional haze condition. Consequently, the turbulent kinetic energy (TKE) is reduced, and the updraft is weakened in the aged-BC cases relative to the clean cases (Figs. 5b, c, h and i), leading to an enhanced atmospheric stratification and hindered development of PBL. The largely reduced TKE during the polluted periods from the model simulations is consistent with field measurements, showing that the turbulent fluxes are greatly reduced in the mixed surface layer under polluted conditions (Wilcox et al., 2016). In addition, surface winds are reduced by 0.7 m s^{-1} from clean to aged-BC cases (Fig. 6b and d), leading to suppressed entrainment aloft and restricted development of the PBL.

The interaction between aerosols and PBL induces further feedbacks at the surface by altering atmospheric dynamic/thermodynamic conditions and stability. For example, the PM concentration at the ground level accumulates when the PBL is compressed, resulting in a smaller extent for vertical dilution. Also, the diurnal feature of PM pollution diminishes because of collapsed PBL, allowing PM to continuously accumulate at the surface. In addition, horizontal advection is also suppressed under polluted conditions, as reflected by weak wind speeds. Consequently, the heavy haze period persists over an extensive period (about 4-7 days) over this region and is only dissipated by strongly northly winds associated with frontal passage (Guo et al., 2014; An et al., 2019). The continuous PM accumulation for multiple days over the NCP is distinct from other megacities across the world, such as Houston, Los Angeles, and Mexico City, which always exhibit a clear diurnal feature of the PM levels (Zhang et al., 2015a), implying a key role of the haze-PBL interaction in deteriorating air quality and worsening the hazy condition in this region. The significant aerosol-PBL interaction and the impact on surface

415 air pollution revealed in our simulation studies are also evident in multiple observation-based
416 studies in China (Dong et al., 2017; Huang et al., 2018; Su et al., 2020). However, there might
417 exist certain uncertainties in evaluating the aerosol impacts on PBL development based on the
418 simulation experiments. Previous observational analysis (Dong et al., 2017; Su et al., 2020)
419 suggestd that the aerosol-PBL interaction also varies with the aerosol vertical structure,
420 compared to an exponential decreasing aerosol profile assumed in our simulations

421 The suppression in PBL height results in significant enhancement of atmospheric
422 moisture, another crucial factor affects the haze evolution, which promotes the occurrence of
423 multiphase reactions (Li et al., 2021a, b). The measured RH increases greatly during the two
424 episodes (Fig. 1d), i.e., from about 18%-19% on the clean days (25 September and 2 October)
425 to 53%-55% on the polluted days (28 September and 5 October). To evaluate the sensitivity of
426 the atmospheric moisture to the PBL height, we employed a modified Nozaki's equation
427 (Nozaki, 1973; Tie et al., 2017) to calculate the RH under different PBL height scenarios using
428 the observed meteorological conditions as inputs (Table 3). The calculated RH increases from
429 29% to 68% for EP1 and from 28% to 73% for EP2, when the PBL height decreases from 1180
430 to 395 m and 1313 to 370 m from clean to polluted days for EP1 and EP2, respectively,
431 indicating that the humidity is highly sensitive to the PBL height.

432 The elevated RH during the polluted period is explained from collapsed PBL to inhibit
433 vertical moisture transport, reduced surface temperature leading to lower saturation vapor
434 pressure, and inefficient entrainment of dry air aloft (Fan et al., 2008; Liu et al., 2013). In
435 addition, enhanced moisture leads to hygroscopic growth of aerosol particles (Liu et al., 2013;
436 Tie et al., 2017). For example, the growth hygroscopic factor relevant to the RH enhancement
437 during EP1 and EP2 increases from 1.3 on the clean days to 1.5 on the hazy days, using an
438 empirical equation derived according to Meier et al. (2009). The additional aerosol growth
439 causes additional attenuation of incoming solar radiation by scattering and absorption to

amplify PBL suppression. Moreover, an enlarged aerosol surface area (due to hygroscopic growth) and elevated RH during the polluted periods favor aqueous-phase reactions to produce sulfate, nitrate, and SOA (Wang et al., 2016a). For example, a recent experimental/field study has shown enhanced sulfate formation, which is catalyzed by BC and increases monotonically from 10% to 70% RH (Zhang et al., 2020). Also, the aqueous reaction of dicarbonyls, which are produced with high yields from oxidation of aromatic VOCs, is significantly enhanced at high RH to yield oligemic products and enhance SOA formation (Li et al., 2021a; b). Hence, enhanced PM production near the ground level strengthens the suppressing effect for the PBL development and results in stabilization and moisture enhancement, constituting positive feedback to amplify the haze development.

3.3.3. The BC effects

We performed model sensitivity simulations to elucidate the role of BC in PBL suppression by considering the non-BC, fresh-BC, and aged-BC scenarios during the polluted periods. Comparison shows a negligible effect on the haze-PBL interaction between the non-BC and fresh-BC cases (Figs. 5, 6 and S5) but large changes in solar radiation and thermodynamic/dynamic conditions within the PBL between the non-BC/ fresh-BC and aged-BC cases, which are attributed to the radiative effects of aged BC. For example, the shortwave heating rate per unit mass is much larger for aged-BC than non-BC and is two times higher for aged-BC than fresh-BC (Figs. 5d and j), suggesting that the BC aging process greatly attenuate incoming solar radiation. Although BC accounts for only 6% of the total aerosol mass under the polluted conditions, about one third of the total reduction in SSR for full-component aerosols is attributed to absorption enhancement after BC aging (Figs. 5f and l). The reduced SSR by the BC aging leads to a cooling of 0.5-0.8 K at the surface. As a result, BC aging contributes significantly to atmospheric stabilization, as evident from weaker updrafts, smaller TKE, and shallower PBL for the aged-BC case (Fig. 5).

The BC aging causes a decrease in the maximum PBL height (at noontime) by about 150 m for the aged-BC case compared to the non-BC and fresh-BC cases. Overall, the BC aging contributes more than 30% of the total reduction in the PBL height by all aerosol components. The restricted PBL development by BC absorption in our work is consistent with that identified previously (Ding et al., 2016; Petäjä et al., 2016). Using a radiative transfer model, Zhang et al. (2020) shows large strongly positive radiative forcing in the atmosphere and strongly negative radiative forcing at the surface by BC aging, consistent with those of the maximal estimates at about noontime from our calculations (Fig. 5i,f). The significant role of BC in atmospheric heating is consistent with long-term observations (Huang et al., 2018), showing that heating in the atmosphere is mainly caused by absorbing aerosols such as BC.

3.4. Aerosol direct radiative forcing

The aerosol direct radiative forcing during regional haze also exhibits a profound climatic effect (Ramanathan et al., 2007). Fig. 7 shows that the total aerosol radiative forcing at the surface (SFC) and in the atmosphere (ATM) during the haze episodes EP1 (EP2) are -87.8 (-62.8) W m^{-2} and 82.2 (56.9) W m^{-2}, respectively. The positive radiative forcing by all aerosols in the atmosphere is dominated by that of aged BC, which accounts for 80% of the total radiative forcing for both episodes. The net radiative forcing at the top of the atmosphere (TOA) by all aerosols for EP1 (EP2) is around -5.6 (-5.9) W m^{-2}, much smaller than the non-BC case with a large negative value of -36.8 (-26.0) W m^{-2}. The strong cooling at the surface is largely canceled out by the strong warming in the atmosphere under the polluted condition, leading to a small net TOA forcing. Clearly, BC aging contributes significantly to cooling at the surface and warming aloft and, hence, the overall radiative budget during the polluted periods. Climatologically, the aerosol TOA forcing on the regional/national level has been shown to be nearly zero or slightly positive in China (Li et al., 2007; Ramanathan et al., 2007; Ding et al., 2016), also demonstrating that the large positive forcing by absorbing aerosols

greatly compensates the negative forcing by the non-absorbing aerosols (Table S1). Therefore, regional global warming is likely mitigated by reducing BC emissions (Wang et al., 2015b).

4. Conclusions

In this work, we analyzed the temporal and spatial characteristics of PM pollution during severe haze events over NCP, by examining ground-based measurements and satellite observations. Severe haze occurs frequently over this region, evident from a periodic (4-7 days) cycle of highly elevated PM pollution. The PM evolutions among the three megacities (Beijing, Baoding and Shijiazhuang) exhibit a remarkable similarity during the haze events, showing nearly synchronized temporal variations in the PM levels. The similar timing and magnitude in the peak $PM_{2.5}$ concentrations among the three megacities indicate significant *in-situ* PM production. Satellite measurements show that the AOD hotspots during the polluted period are co-located with the three megacities, but are distinct from seasonal and annual AOD means, indicating the importance of urban emissions (mainly traffic emissions consisting of anthropogenic VOCs and NO_x). *In-situ* PM production occurs most efficiently over the megacities, and urban sources relevant to traffic emissions play a critical role in regional severe haze formation.

Our result reveals that the rapid photochemistry drives the PM production during the transition period. There exist concurrent increases in OOA and $PM_{2.5}$ concentrations and a strong correlation between OOA and O_x concentrations during this period. The [OOA]/[Ox] ratio in Beijing is much higher than that in Mexico City and Houston, attributable to much higher level of gaseous precursors (i.e., anthropogenic VOCs and NO_x) in Beijing than the other two cities. The correlation between [OOA] and [O_x], however, vanishes during the polluted period, when O_3 production is significantly suppressed because of reduced solar ultraviolet radiation and inefficient photooxidation (Wu et al., 2020; Peng et al., 2021). The continuing increases in $PM_{2.5}$ and OOA with decreasing O_x during the polluted period implies

a key role of multiphase chemistry in driving the haze severity, when the RH level is significantly elevated. The continuous growth in $PM_{2.5}$ and OOA during the polluted period has been explained by an increasing importance of heterogeneous chemistry to contribute to sulfate, nitrate, and SOA formation (Wang et al., 2016a; An et al., 2019; Peng et al., 2021; Zhang et al., 2021).

Using the WRF model coupled with an explicit aerosol radiative module, we elucidated the underlying mechanism relevant to the haze-PBL interactions, showing a positive feedback to haze formation at the ground level. The PBL height is largely reduced under the polluted condition, since the PBL is markedly suppressed (as indicated by the reduced TKE and weakened updraft), because of strong aerosol heating in the atmosphere and strong cooling at the surface. The PM concentration near the surface accumulates significantly in a compressed PBL, since PM dispersion is unfavorable in the stratified and collapsed PBL, leading to continuous growth and accumulation of PM over multiple days. Calculations using the modified Nozaki's equation shows that the suppressed PBL results in a great enhancement of atmospheric moisture near the surface. A more humid condition leads to hygroscopic growth of aerosol particles and more efficient multiphase PM production. Therefore, haze development near the surface is considerably exacerbated because of the positive feedback in responding to the atmospheric moisture and thermodynamic/dynamic conditions to amplify the haze severity.

Our combined observational analysis of the temporal/spatial PM distributions and modeling unravel a dominant regional characteristic for severe haze evolution in the NCP region, showing rapid *in-situ* PM production and inefficient transport, both of which are amplified by air stabilization. On the other hand, regional transport sufficiently disperses the gaseous aerosol precursors (SO_2, NO_x, VOCs, and NH_3) during the clean period, which subsequently result in rapid *in-situ* PM production via photochemistry during the transition period and via multiphase chemistry during the polluted period.

The modeling simulations on two haze episodes indicate important regional climatic effects. The net TOA forcing for the two hazy days is about of -5.6 ~ -5.9 W m^{-2}, showing strong negative radiative forcing (cooling) of -63 to -88 W m^{-2} at the surface and strong positive radiative forcing (warming) of 57 to 82 W m^{-2} in the atmosphere. BC represents the dominant contributor to the positive aerosol radiative forcing in the atmosphere, thus playing a significant role in the haze-PBL interaction. Specifically, BC aging contributes to more than 30% of the PBL collapse induced by total aerosols and about 50% of the TOA positive radiative forcing. Our work highlights the necessity to better understand the BC aging process and improve representation in atmospheric models for accurate assessment of the aerosol climatic effects. We conclude that reduction in BC emissions achieves co-benefits, which improve local and regional air quality by minimizing air stagnation and mitigate the global warming by alleviating the positive direct radiative forcing.

Code and data availability

The source code of WRF was similar to that described previously by Li et al., (2008) and Fan et al. (2008). All data employed in the present study were described in section 2.1 and were also available from the author (Y.L.) upon request.

Supplement

The supplement related to this article is available online at: https://doi.org/10.5194/acp-22-xxxx-supplement

Author contributions

RZ created the original research framework and provided research direction. YL and YW developed the model theory, co-wrote the software, established a database, analyzed the data, and created the figures. All authors analyzed the data and co-wrote the manuscript.

Disclaimer

Publisher's note: Copernicus Publications remains neutral with regard to jurisdictional claims in published maps and institutional affiliations.

Acknowledgements

This work was supported by a collaborative Program between the Texas A&M University (TAMU) and the Natural Science Foundation of China (NSFC). R.Z. acknowledged additional support by the Robert A. Welch Foundation (Grant A-1417). The modeling portion of this research was conducted at the TAMU High Performance Research Computing. We thanked Hong-Bin Chen and Philippe Goloub for the data at the Beijing AERONET site.

References

Aiken, A. C., Salcedo, D., Cubison, M. J., Huffman, J. A., DeCarlo, P. F., Ulbrich, I. M., Docherty, K. S., Sueper, D., Kimmel, J. R., Worsnop, D. R., Trimborn, A., Northway, M., Stone, E. A., Schauer, J. J., Volkamer, R. M., Fortner, E., de Foy, B., Wang, J., Laskin, A., Shutthanandan, V., Zheng, J., Zhang, R., Gaffney, J., Marley, N. A., Paredes-Miranda, G., Arnott, W. P., Molina, L. T., Sosa, G., and Jimenez, J. L.: Mexico City aerosol analysis during MILAGRO using high resolution aerosol mass spectrometry at the urban supersite (T0) – Part 1: Fine particle composition and organic source apportionment, Atmos. Chem. Phys., 9, 6633–6653, https://doi.org/10.5194/acp-9-6633-2009, 2009.

An, Z. S., Huang, R. J., Zhang, R. Y., Tie, X. X., Li, G. H., Cao, J. J., Zhou, W. J., Shi, Z. G., Han, Y. M., Gu, Z. L., and Ji, Y. M.: Severe haze in northern China: A synergy of anthropogenic emissions and atmospheric processes, Proc. Natl. Acad. Sci. USA, 116, 8657-8666, 10.1073/pnas.1900125116, 2019.

Atkinson, R.: Atmospheric chemistry of VOCs and NOx, Atmos. Environ., 34, 2063-2101, http://dx.doi.org/10.1016/S1352-2310(99)00460-4, 2000.

Bond, T. C., Doherty, S. J., Fahey, D. W., Forster, P. M., Berntsen, T., DeAngelo, B. J., Flanner, M. G., Ghan, S., Kärcher, B., Koch, D., Kinne, S., Kondo, Y., Quinn, P. K., Sarofim, M. C., Schultz, M. G., Schulz, M., Venkataraman, C., Zhang, H., Zhang, S., Bellouin, N., Guttikunda, S. K., Hopke, P. K., Jacobson, M. Z., Kaiser, J. W., Klimont, Z., Lohmann, U., Schwarz, J. P., Shindell, D., Storelvmo, T., Warren, S. G., and Zender, C. S.: Bounding the role of black carbon in the climate system: A scientific assessment, J. Geophys. Res.: Atmos., 118, 5380-5552, 10.1002/jgrd.50171, 2013.

597 Bouarar, I., Wang, X. M., and Brasseur, G. P.: Air Pollution in Eastern Asia: An Integrated
598 Perspective Preface, Issi Sci Rep Ser, 16, V-Viii, Book_Doi 10.1007/978-3-319-59489-7,
599 2017.
600 Cai, W., Li, K., Liao, H., Wang, H., and Wu, L.: Weather conditions conducive to Beijing
601 severe haze more frequent under climate change, Nature Clim. Change, 7, 257,
602 10.1038/nclimate3249, 2017.
603 Che, H., Xia, X., Zhu, J., Li, Z., Dubovik, O., Holben, B., Goloub, P., Chen, H., Estelles, V.,
604 Cuevas-Agullo, E., Blarel, L., Wang, H., Zhao, H., Zhang, X., Wang, Y., Sun, J., Tao, R.,
605 Zhang, X., and Shi, G.: Column aerosol optical properties and aerosol radiative forcing
606 during a serious haze-fog month over North China Plain in 2013 based on ground-based
607 sunphotometer measurements, Atmos. Chem. Phys., 14, 2125-2138, 10.5194/acp-14-
608 2125-2014, 2014.
609 Ding, A. J., Huang, X., Nie, W., Sun, J. N., Kerminen, V. M., Petäjä, T., Su, H., Cheng, Y.
610 F., Yang, X. Q., Wang, M. H., Chi, X. G., Wang, J. P., Virkkula, A., Guo, W. D., Yuan,
611 J., Wang, S. Y., Zhang, R. J., Wu, Y. F., Song, Y., Zhu, T., Zilitinkevich, S., Kulmala,
612 M., and Fu, C. B.: Enhanced haze pollution by black carbon in megacities in China,
613 Geophys. Res. Lett., 43, 2873–2879, 10.1002/2016GL067745, 2016.
614 Dong, Z., Li, Z., Yu, X., Cribb, M., Li, X., and Dai, J.: Opposite long-term trends in aerosols
615 between low and high altitudes: a testimony to the aerosol–PBL feedback, Atmos. Chem.
616 Phys., 17, 7997–8009, https://doi.org/10.5194/acp-17-7997-2017, 2017.
617 Fan, J., and Zhang, R. Atmospheric oxidation mechanism of isoprene. Environ. Chem., 1,
618 140-149, 2004.
619 Fan, J., Zhang, R., Tao, W.-K., and Mohr, K. I.: Effects of aerosol optical properties on deep
620 convective clouds and radiative forcing, J. Geophys. Res., 113, D08209,
621 10.1029/2007jd009257, 2008.

622 Guo, S., Hu, M., Zamora, M. L., Peng, J., Shang, D., Zheng, J., Du, Z., Wu, Z., Shao, M.,
623 Zeng, L., Molina, M. J., and Zhang, R.: Elucidating severe urban haze formation in
624 China, Proc. Natl. Acad. Sci. U S A, 111, 17373-17378, 10.1073/pnas.1419604111, 2014.
625 Guo, S., Hu, M., Peng, J. F., Wu, Z. J., Zamora, M. L., Shang, D. J., Du, Z. F., Zheng, J.,
626 Fang, X., Tang, R. Z., Wu, Y. S., Zeng, L. M., Shuai, S. J., Zhang, W. B., Wang, Y., Ji,
627 Y. M., Li, Y. X., Zhang, A. L., Wang, W. G., Zhang, F., Zhao, J. Y., Gong, X. L., Wang,
628 C. Y., Molina, M. J., and Zhang, R. Y.: Remarkable nucleation and growth of ultrafine
629 particles from vehicular exhaust, Proc. Natl. Acad. Sci. USA, 117, 3427-3432,
630 10.1073/pnas.1916366117, 2020.
631 Guo, S., Hu, M., Lin, Y., Gomez-Hernandez, M., Zamora, M. L., Peng, J. F., Collins, D. R.,
632 and Zhang, R. Y.: OH-Initiated Oxidation of m-Xylene on Black Carbon Aging, Environ.
633 Sci. Technol., 50, 8605-8612, 10.1021/acs.est.6b01272, 2016.
634 Gustafsson, Ö., and Ramanathan, V.: Convergence on climate warming by black carbon
635 aerosols, Proc. Natl. Acad. Sci. USA, 113, 4243-4245, 10.1073/pnas.1603570113, 2016.
636 He, C., Liou, K. N., Takano, Y., Zhang, R., Levy Zamora, M., Yang, P., Li, Q., and Leung, L.
637 R.: Variation of the radiative properties during black carbon aging: theoretical and
638 experimental intercomparison, Atmos. Chem. Phys., 15, 11967-11980, 10.5194/acp-15-
639 11967-2015, 2015.
640 Huang, X., Wang, Z., and Ding, A.: Impact of Aerosol-PBL Interaction on Haze Pollution:
641 Multiyear Observational Evidences in North China, Geophys. Res. Lett., 45, 8596–8603,
642 https://doi.org/10.1029/2018GL079239, 2018.
643 Intergovernmental Panel on Climate Change (IPCC). *Climate Change 2013: The Physical*
644 *Science Basis. Contribution of Working Group I to the Fifth Assessment Report of the*
645 *Intergovernmental Panel on Climate Change*. Cambridge University Press, **2013**.

646 Ji, Y., J. Zhao, H. Terazono, K. Misawa, N. P. Levitt, Y. Li, Y. Lin, J. Peng, Y. Wang, L.
647 Duan, B. Pan, F. Zhang, X. Feng, T. An, W. Marrero-Ortiz, J. Secrest, A.L. Zhang, K.
648 Shibuya, M. J. Molina, and R. Zhang, Reassessing the atmospheric oxidation mechanism
649 of toluene, Proc. Natl. Acad. Sci. USA, 114, 8169–8174, DOI:10.1073/pnas.1705463114,
650 2017.

651 Ji, Y., Q. Shi, Y. Li, T. An, J. Zheng, J. Peng, Y. Gao, J. Chen, G. Li, Y. Wang, F. Zhang,
652 A.L. Zhang, J. Zhao, M. J. Molina, and R. Zhang, Carbenium ion-mediated
653 oligomerization of methylglyoxal for secondary organic aerosol formation, Proc. Natl.
654 Acad. Sci. USA, 117, 13294-13299, doi.org/10.1073/pnas.1912235117, 2020.

655 Ji, Y., Q. Shi, Y. Li[#], T. An, J. Zheng, J. Peng, Y. Gao, J. Chen, G. Li, Y. Wang, F. Zhang,
656 A.L. Zhang, J. Zhao[#], M. J. Molina, and **R. Zhang**, Carbenium ion-mediated
657 oligomerization of methylglyoxal for secondary organic aerosol formation, *Proc. Natl.*
658 *Acad. Sci. USA* **117**, 13294-13299, doi.org/10.1073/pnas.1912235117 (2020).

659 Khalizov, A. F., Lin, Y., Qiu, C., Guo, S., Collins, D., and Zhang, R.: Role of OH-initiated
660 oxidation of isoprene in aging of combustion soot, Environ. Sci. Technol., 47, 2254-2263,
661 10.1021/es3045339, 2013.

662 Johnson, N. M., Hoffmann, A. R., Behlen, J. C., Lau, C., Pendleton, D., Harvey, N., Shore,
663 R., Li, Y. X., Chen, J. S., Tian, Y. A., and Zhang, R. Y.: Air pollution and children's
664 health-a review of adverse effects associated with prenatal exposure from fine to ultrafine
665 particulate matter, Environ. Health. Prev., 26, ARTN 72, 10.1186/s12199-021-00995-5,
666 2021.

667 Lee, S.-H., Gordon, H., Yu, H., Lehtipalo, K., Haley, R., Li, Y., Zhang, R.: New Particle
668 Formation in the Atmosphere: From Molecular Clusters to Global Climate, J. Geophys.
669 Res. Atmos., 124, 7098-7146, doi.org: 10.1029/2018JD029356, 2019.

Levy, R. C., Leptoukh, G. G., Kahn, R., Zubko, V., Gopalan, A., and Remer, L. A.: A Critical Look at Deriving Monthly Aerosol Optical Depth From Satellite Data, Ieee T Geosci Remote, 47, 2942-2956, Doi 10.1109/Tgrs.2009.2013842, 2009.

Li, G., Wang, Y., and Zhang, R.: Implementation of a two-moment bulk microphysics scheme to the WRF model to investigate aerosol-cloud interaction, J. Geophys. Res., 113, D15211, 10.1029/2007jd009361, 2008.

Li, P., Yan, R., Yu, S., Wang, S., Liu, W., and Bao, H.: Reinstate regional transport of PM2.5 as a major cause of severe haze in Beijing, Proc. Natl. Acad. Sci. USA, 112, E2739-E2740, 10.1073/pnas.1502596112, 2015.

Li, Y., Zhao, J., Wang, Y., Seinfeld, J. H., and Zhang, R.: Multigeneration Production of Secondary Organic Aerosol from Toluene Photooxidation, Environmental science & technology, 55, 8592-8603, 10.1021/acs.est.1c02026, 2021a.

Li, Y., Ji, Y., Zhao, J., Wang, Y., Shi, Q., Peng, J., Wang, Y., Wang, C., Zhang, F., Wang, Y., Seinfeld, J. H., and Zhang, R.: Unexpected Oligomerization of Small α-Dicarbonyls for Secondary Organic Aerosol and Brown Carbon Formation, Environmental science & technology, 55, 4430-4439, 10.1021/acs.est.0c08066, 2021b.

Li, Z., Xia, X., Cribb, M., Mi, W., Holben, B., Wang, P., Chen, H., Tsay, S.-C., Eck, T. F., Zhao, F., Dutton, E. G., and Dickerson, R. E.: Aerosol optical properties and their radiative effects in northern China, J. Geophys. Res.: Atmos., 112, D22S01, 10.1029/2006JD007382, 2007.

Li, Z., Guo, J., Ding, A., Liao, H., Liu, J., Sun, Y., Wang, T., Xue, H., Zhang, H., and Zhu, B.: Aerosol and Boundary-Layer Interactions and Impact on Air Quality, Natl. Sci. Rev., nwx117-nwx117, 10.1093/nsr/nwx117, 2017.

Li, Z. Q., Wang, Y., Guo, J. P., Zhao, C. F., Cribb, M., Dong, X. Q., Fan, J. W., Gong, D. Y., Huang, J. P., Jiang, M. J., Jiang, Y. Q., Lee, S. S., Li, H., Li, J. M., Liu, J. J., Qian, Y.,

695 Rosenfeld, D., Shan, S. Y., Sun, Y. L., Wang, H. J., Xin, J. Y., Yan, X., Yang, X., Yang,
696 X. Q., Zhang, F., and Zheng, Y. T.: East Asian Study of Tropospheric Aerosols and their
697 Impact on Regional Clouds, Precipitation, and Climate (EAST-AIR(CPC)), J. Geophys.
698 Res.-Atmos., 124, 13026-13054, 10.1029/2019jd030758, 2019.
699 Lin, Y., Wang, Y., Pan, B., Hu, J., Liu, Y., and Zhang, R.: Distinct Impacts of Aerosols on an
700 Evolving Continental Cloud Complex during the RACORO Field Campaign, J. Atmos.
701 Sci., 73, 3681-3700, doi:10.1175/JAS-D-15-0361.1, 2016.
702 Liu, J., F. Zhang, W. Xu, Y. Sun, L. Chen, S. Li, J. Ren, B. Hu, H. Wu, and R. Zhang,
703 Hygroscopicity of organic aerosols linked to formation mechanisms. Geophy. Res. Lett.
704 48, doi.org/10.1029/2020GL091683, 2021.
705 Liu, X. G., Li, J., Qu, Y., Han, T., Hou, L., Gu, J., Chen, C., Yang, Y., Liu, X., Yang, T.,
706 Zhang, Y., Tian, H., and Hu, M.: Formation and evolution mechanism of regional haze: a
707 case study in the megacity Beijing, China, Atmos. Chem. Phys., 13, 4501-4514, DOI
708 10.5194/acp-13-4501-2013, 2013.
709 Mallet, M., Roger, J. C., Despiau, S., Putaud, J. P., and Dubovik, O.: A study of the mixing
710 state of black carbon in urban zone, J. Geophys. Res.: Atmos., 109, n/a-n/a,
711 10.1029/2003JD003940, 2004.
712 Meier, J., Wehner, B., Massling, A., Birmili, W., Nowak, A., Gnauk, T., Brüggemann, E.,
713 Herrmann, H., Min, H., and Wiedensohler, A.: Hygroscopic growth of urban aerosol
714 particles in Beijing (China) during wintertime: a comparison of three experimental
715 methods, Atmos. Chem. Phys., 9, 6865-6880, 10.5194/acp-9-6865-2009, 2009.
716 Menon, S., Hansen, J., Nazarenko, L., and Luo, Y.: Climate Effects of Black Carbon
717 Aerosols in China and India, Science, 297, 2250-2253, 10.1126/science.1075159, 2002.
718 Molina, L. T.: Introductory lecture: air quality in megacities, Faraday Discuss, 226, 9-52,
719 10.1039/d0fd00123f, 2021.

720 Nozaki, K. Y.: Mixing Depth Model Using Hourly Surface Observations Report 7053, USAF
721 Environmental Technical Applications Center, 1973.
722 Pasquill, F.: The Estimation of the Dispersion of Windborne Material, Meteorological
723 Magazin, 90, 33-49, 1961.
724 Peng, J., Hu, M., Guo, S., Du, Z., Zheng, J., Shang, D., Levy Zamora, M., Zeng, L., Shao,
725 M., Wu, Y.-S., Zheng, J., Wang, Y., Glen, C. R., Collins, D. R., Molina, M. J., and
726 Zhang, R.: Markedly enhanced absorption and direct radiative forcing of black carbon
727 under polluted urban environments, Proc. Natl. Acad. Sci. USA, 4266–4271,
728 10.1073/pnas.1602310113, 2016.
729 Peng, J., Hu, M., Guo, S., Du, Z., Shang, D., Zheng, J., Zheng, J., Zeng, L., Shao, M., Wu,
730 Y., Collins, D., and Zhang, R.: Ageing and hygroscopicity variation of black carbon
731 particles in Beijing measured by a quasi-atmospheric aerosol evolution study
732 (QUALITY) chamber, Atmos. Chem. Phys., 17, 10333-10348, 10.5194/acp-17-10333-
733 2017, 2017.
734 Peng, J. F., Hu, M., Shang, D. J., Wu, Z. J., Du, Z. F., Tan, T. Y., Wang, Y. N., Zhang, F.,
735 and Zhang, R. Y.: Explosive Secondary Aerosol Formation during Severe Haze in the
736 North China Plain, Environ. Sci. Technol., 55, 2189-2207, 10.1021/acs.est.0c07204,
737 2021.
738 Petäjä, T., Järvi, L., Kerminen, V. M., Ding, A. J., Sun, J. N., Nie, W., Kujansuu, J.,
739 Virkkula, A., Yang, X., Fu, C. B., Zilitinkevich, S., and Kulmala, M.: Enhanced air
740 pollution via aerosol-boundary layer feedback in China, Sci. Rep., 6, 18998,
741 10.1038/srep18998, 2016.
742 Qian, Y., Leung, R.L., Ghan, S. J., and Giorgi, F.: Regional climate effects of aerosols over
743 China: modeling and observation, Tellus B, 55, 914-934, 10.1046/j.1435-
744 6935.2003.00070.x, 2003.

745 Qian, Y, Gong, D., Fan, J., Leung, R.L., Bennartz, R., Chen, D., Wang, W.: Heavy pollution
746 suppresses light rain in China: Observations and modeling, J. Geophys. Res.: Atmos.,
747 114, 10.1029/2008JD011575, 2009.
748 Ramanathan, V., Li, F., Ramana, M. V., Praveen, P. S., Kim, D., Corrigan, C. E., Nguyen, H.,
749 Stone, E. A., Schauer, J. J., Carmichael, G. R., Adhikary, B., and Yoon, S. C.:
750 Atmospheric brown clouds: Hemispherical and regional variations in long-range
751 transport, absorption, and radiative forcing, J. Geophys. Res.: Atmos., 112, D22S21,
752 10.1029/2006JD008124, 2007.
753 Rychlik, K. A., Secrest, J. R., Lau, C., Pulczinski, J., Zamora, M. L., Leal, J., Langley, R.,
754 Myatt, L. G., Raju, M., Chang, R. C. A., Li, Y. X., Golding, M. C., Rodrigues-Hoffmann,
755 A., Molina, M. J., Zhang, R. Y., and Johnson, N. M.: In utero ultrafine particulate matter
756 exposure causes offspring pulmonary immunosuppression, Proc. Natl. Acad. Sci. USA,
757 116, 3443-3448, 10.1073/pnas.1816103116, 2019.
758 Su, T., Li, Z., Li, C., Li, J., Han, W., Shen, C., Tan, W., Wei, J., and Guo, J.: The significant
759 impact of aerosol vertical structure on lower atmosphere stability and its critical role in
760 aerosol–planetary boundary layer (PBL) interactions, Atmos. Chem. Phys., 20, 3713–
761 3724, https://doi.org/10.5194/acp-20-3713-2020, 2020.
762 Suh, I., Lei, W., and Zhang, R. Experimental and theoretical studies of isoprene reaction with
763 NO_3. J. Phys. Chem. 105, 6471-6478, 2001.
764 Sun, Y. L., Jiang, Q., Wang, Z. F., Fu, P. Q., Li, J., Yang, T., and Yin, Y.: Investigation of
765 the Sources and Evolution Processes of Severe Haze Pollution in Beijing in January 2013,
766 J. Geophys Res.-Atmos., 119, 4380-4398, Doi 10.1002/2014jd021641, 2014.
767 Tang, G., Zhang, J., Zhu, X., Song, T., Münkel, C., Hu, B., Schäfer, K., Liu, Z., Zhang, J.,
768 Wang, L., Xin, J., Suppan, P., and Wang, Y.: Mixing layer height and its implications for

air pollution over Beijing, China, Atmos. Chem. Phys., 16, 2459-2475, 10.5194/acp-16-2459-2016, 2016a.

Tang, W., Qin, J., Yang, K., Liu, S., Lu, N., and Niu, X.: Retrieving high-resolution surface solar radiation with cloud parameters derived by combining MODIS and MTSAT data, Atmos. Chem. Phys., 16, 2543-2557, 10.5194/acp-16-2543-2016, 2016b.

Tie, X., Huang, R.-J., Cao, J., Zhang, Q., Cheng, Y., Su, H., Chang, D., Pöschl, U., Hoffmann, T., Dusek, U., Li, G., Worsnop, D. R., and O'Dowd, C. D.: Severe Pollution in China Amplified by Atmospheric Moisture, Sci. Rep., 7, 15760, 10.1038/s41598-017-15909-1, 2017.

Wallace, J. M., and Hobbs, P. V.: Atmospheric Science, Second Edition, Elsevier, 2005.

Wang, G., Zhang, R., Gomez, M. E., Yang, L., Levy Zamora, M., Hu, M., Lin, Y., Peng, J., Guo, S., Meng, J., Li, J., Cheng, C., Hu, T., Ren, Y., Wang, Y., Gao, J., Cao, J., An, Z., Zhou, W., Li, G., Wang, J., Tian, P., Marrero-Ortiz, W., Secrest, J., Du, Z., Zheng, J., Shang, D., Zeng, L., Shao, M., Wang, W., Huang, Y., Wang, Y., Zhu, Y., Li, Y., Hu, J., Pan, B., Cai, L., Cheng, Y., Ji, Y., Zhang, F., Rosenfeld, D., Liss, P. S., Duce, R. A., Kolb, C. E., and Molina, M. J.: Persistent sulfate formation from London Fog to Chinese haze, Proc. Natl. Acad. Sci. USA, 113, 13630-13635, 10.1073/pnas.1616540113, 2016a.

Wang, H., Shi, G. Y., Zhang, X. Y., Gong, S. L., Tan, S. C., Chen, B., Che, H. Z., and Li, T.: Mesoscale modelling study of the interactions between aerosols and PBL meteorology during a haze episode in China Jing–Jin–Ji and its near surrounding region – Part 2: Aerosols' radiative feedback effects, Atmos. Chem. Phys., 15, 3277-3287, 10.5194/acp-15-3277-2015, 2015a.

Wang, J., Allen, D. J., Pickering, K. E., Li, Z., and He, H.: Impact of aerosol direct effect on East Asian air quality during the EAST-AIRE campaign, J. Geophys. Res.: Atmos., 121, 6534-6554, 10.1002/2016JD025108, 2016b.

794 Wang, Y., Wan, Q., Meng, W., Liao, F., Tan, H., and Zhang, R.: Long-term impacts of
795 aerosols on precipitation and lightning over the Pearl River Delta megacity area in China,
796 Atmos. Chem. Phys., 11, 12421-12436, 10.5194/acp-11-12421-2011, 2011.
797 Wang, Y., Che, H., Ma, J., Wang, Q., Shi, G., Chen, H., Goloub, P., and Hao, X.: Aerosol
798 radiative forcing under clear, hazy, foggy, and dusty weather conditions over Beijing,
799 China, Geophys. Res. Lett., 36, n/a-n/a, 10.1029/2009GL037181, 2009.
800 Wang, Y., Khalizov, A., Levy, M., and Zhang, R. Y.: New Directions: Light absorbing
801 aerosols and their atmospheric impacts, Atmos. Environ., 81, 713-715,
802 10.1016/j.atmosenv.2013.09.034, 2013.
803 Wang, Y., Zhang, R., and Saravanan, R.: Asian pollution climatically modulates mid-latitude
804 cyclones following hierarchical modelling and observational analysis, Nat. commun., 5,
805 3098, 10.1038/ncomms4098, 2014a.
806 Wang, Y., Wang, M., Zhang, R., Ghan, S. J., Lin, Y., Hu, J., Pan, B., Levy, M., Jiang, J. H.,
807 and Molina, M. J.: Assessing the effects of anthropogenic aerosols on Pacific storm track
808 using a multiscale global climate model, Proc. Natl. Acad. Sci. U S A, 111, 6894-6899,
809 10.1073/pnas.1403364111, 2014b.
810 Wang, Y., Lee, K.-H., Lin, Y., Levy, M., and Zhang, R.: Distinct effects of anthropogenic
811 aerosols on tropical cyclones, Nature Clim. Change, 4, 368-373, 10.1038/nclimate2144,
812 2014c.
813 Wang, Y. S., Yao, L., Wang, L. L., Liu, Z. R., Ji, D. S., Tang, G. Q., Zhang, J. K., Sun, Y.,
814 Hu, B., and Xin, J. Y.: Mechanism for the Formation of the January 2013 Heavy Haze
815 Pollution Episode over Central and Eastern China, Sci. China Earth Sci., 57, 14-25, DOI
816 10.1007/s11430-013-4773-4, 2014d.

817 Wang, Z., Huang, X., and Ding, A.: Dome effect of black carbon and its key influencing
818 factors: A one-dimensional modelling study, Atmos. Chem. Phys. Discuss., 2017, 1-29,
819 10.5194/acp-2017-967, 2017.
820 Wang, Z. L., Zhang, H., and Zhang, X. Y.: Simultaneous reductions in emissions of black
821 carbon and co-emitted species will weaken the aerosol net cooling effect, Atmos. Chem.
822 Phys., 15, 3671-3685, 10.5194/acp-15-3671-2015, 2015b.
823 Wilcox, E. M., Thomas, R. M., Praveen, P. S., Pistone, K., Bender, F. A.-M., and
824 Ramanathan, V.: Black carbon solar absorption suppresses turbulence in the atmospheric
825 boundary layer, Proc. Natl. Acad. Sci. USA, 113, 11794-11799,
826 10.1073/pnas.1525746113, 2016.
827 Wood, E. C., Canagaratna, M. R., Herndon, S. C., Onasch, T. B., Kolb, C. E., Worsnop, D.
828 R., Kroll, J. H., Knighton, W. B., Seila, R., Zavala, M., Molina, L. T., DeCarlo, P. F.,
829 Jimenez, J. L., Weinheimer, A. J., Knapp, D. J., Jobson, B. T., Stutz, J., Kuster, W. C.,
830 and Williams, E. J.: Investigation of the correlation between odd oxygen and secondary
831 organic aerosol in Mexico City and Houston, Atmos. Chem. Phys., 10, 8947-8968,
832 10.5194/acp-10-8947-2010, 2010.
833 Wu, G., Li, Z., Fu, C., Zhang, X., Zhang, R., Zhang, R., Zhou, T., Li, J., Li, J., Zhou, D., Wu,
834 L., Zhou, L., He, B. and Huang, R. Advances in studying interactions between aerosols
835 and monsoon in China, *Sci.* China: Earth Sci., 59, 1–16, 10.1007/s11430-015-5198-z,
836 2016.
837 Wu, G. Y., Brown, J., Zamora, M. L., Miller, A., Satterfield, M. C., Meininger, C. J.,
838 Steinhauser, C. B., Johnson, G. A., Burghardt, R. C., Bazer, F. W., Li, Y. X., Johnson, N.
839 M., Molina, M. J., and Zhang, R. Y.: Adverse organogenesis and predisposed long-term
840 metabolic syndrome from prenatal exposure to fine particulate matter, Proc. Natl. Acad.
841 Sci. USA, 116, 11590-11595, 10.1073/pnas.1902925116, 2019.

Wu, J. R., Bei, N. F., Hu, B., Liu, S. X., Wang, Y., Shen, Z. X., Li, X., Liu, L., Wang, R. N., Liu, Z. R., Cao, J. J., Tie, X. X., Molina, L. T., and Li, G. H.: Aerosol-photolysis interaction reduces particulate matter during wintertime haze events, Proc. Natl. Acad. Sci. USA, 117, 9755-9761, 10.1073/pnas.1916775117, 2020.

Xia, X., Chen, H., Goloub, P., Zhang, W., Chatenet, B., and Wang, P.: A compilation of aerosol optical properties and calculation of direct radiative forcing over an urban region in northern China, J. Geophys. Res.: Atmos., 112, 10.1029/2006JD008119, 2007.

Xu, W., and Zhang, R.: Theoretical investigation of interaction of dicarboxylic acids with common aerosol nucleation precursors, J. Phys. Chem., 116, 4539-4550, doi: 10.1021/jp301964u, 2012.

Yuan, T., Li, Z., Zhang, R., and Fan, J. Increase of cloud droplet size with aerosol optical depth: An observation and modeling study, J. Geophys. Res., 113, D04201, doi:10.1029/2007JD008632, 2008.

Zhang, F., Wang, Y., Peng, J. F., Chen, L., Sun, Y. L., Duan, L., Ge, X. L., Li, Y. X., Zhao, J. Y., Liu, C., Zhang, X. C., Zhang, G., Pan, Y. P., Wang, Y. S., Zhang, A. L., Ji, Y. M., Wang, G. H., Hu, M., Molina, M. J., and Zhang, R. Y.: An unexpected catalyst dominates formation and radiative forcing of regional haze, Proc. Natl. Acad. Sci. USA, 117, 3960-3966, doi/10.1073/pnas.1919343117, 2020.

Zhang, R., Li, G. H., Fan, J. W., Wu, D. L., and Molina, M. J.: Intensification of Pacific storm track linked to Asian pollution, Proc. Natl. Acad. Sci. USA, 104, 5295-5299, 10.1073/pnas.0700618104, 2007.

Zhang, R., Wang, L., Khalizov, A. F., Zhao, J., Zheng, J., McGraw, R. L. and Molina, L. T.: Formation of nanoparticles of blue haze enhanced by anthropogenic pollution, Proc. Natl. Acad. Sci. USA, 106, 17650-17654, doi:10.1073/pnas.0910125106, 2009.

Zhang, R., Khalizov, A. F., Pagels, J., Zhang, D., Xue, H., and McMurry, P. H.: Variability in morphology, hygroscopicity, and optical properties of soot aerosols during atmospheric processing, Proc. Natl. Acad. Sci. USA, 105, 10291-10296, 10.1073/pnas.0804860105, 2008.

Zhang, R., Wang, G., Guo, S., Zamora, M. L., Ying, Q., Lin, Y., Wang, W., Hu, M., and Wang, Y.: Formation of Urban Fine Particulate Matter, Chem. Rev., 115, 3803-3855, 10.1021/acs.chemrev.5b00067, 2015a.

Zhang, R., Guo, S., Levy Zamora, M., and Hu, M.: Reply to Li et al.: Insufficient evidence for the contribution of regional transport to severe haze formation in Beijing, Proc. Natl. Acad. Sci. USA, 112, E2741, 10.1073/pnas.1503855112, 2015b.

Zhang, R., N.M. Johnson, Y. Li: Establishing the exposure-outcome relation between airborne particulate matter and children's health, Thorax, 76, doi.org/10.1136/thoraxjnl-2021- 217017, 2021.

Zhang, X., Zhang, Q., Hong, C., Zheng, Y., Geng, G., Tong, D., Zhang, Y., and Zhang, X.: Enhancement of PM2.5 concentrations by aerosol-meteorology interactions over China, J. Geophys. Res.: Atmos., 1179-1194, 10.1002/2017JD027524, 2018.

Zhao, J., Zhang, R., Fortner, E.C., and North, S.W.: Quantification of hydroxycarbonyls from OH-isoprene reactions, J. Am. Chem. Soc., 126, 2686-2687, 2004.

Zhao, J., Zhang, R., Misawa, K. and Shibuya, K. Experimental product study of the OH-initiated oxidation of m-xylene. J. Photoch. Photobio. A, 176, 199-207, 2005.

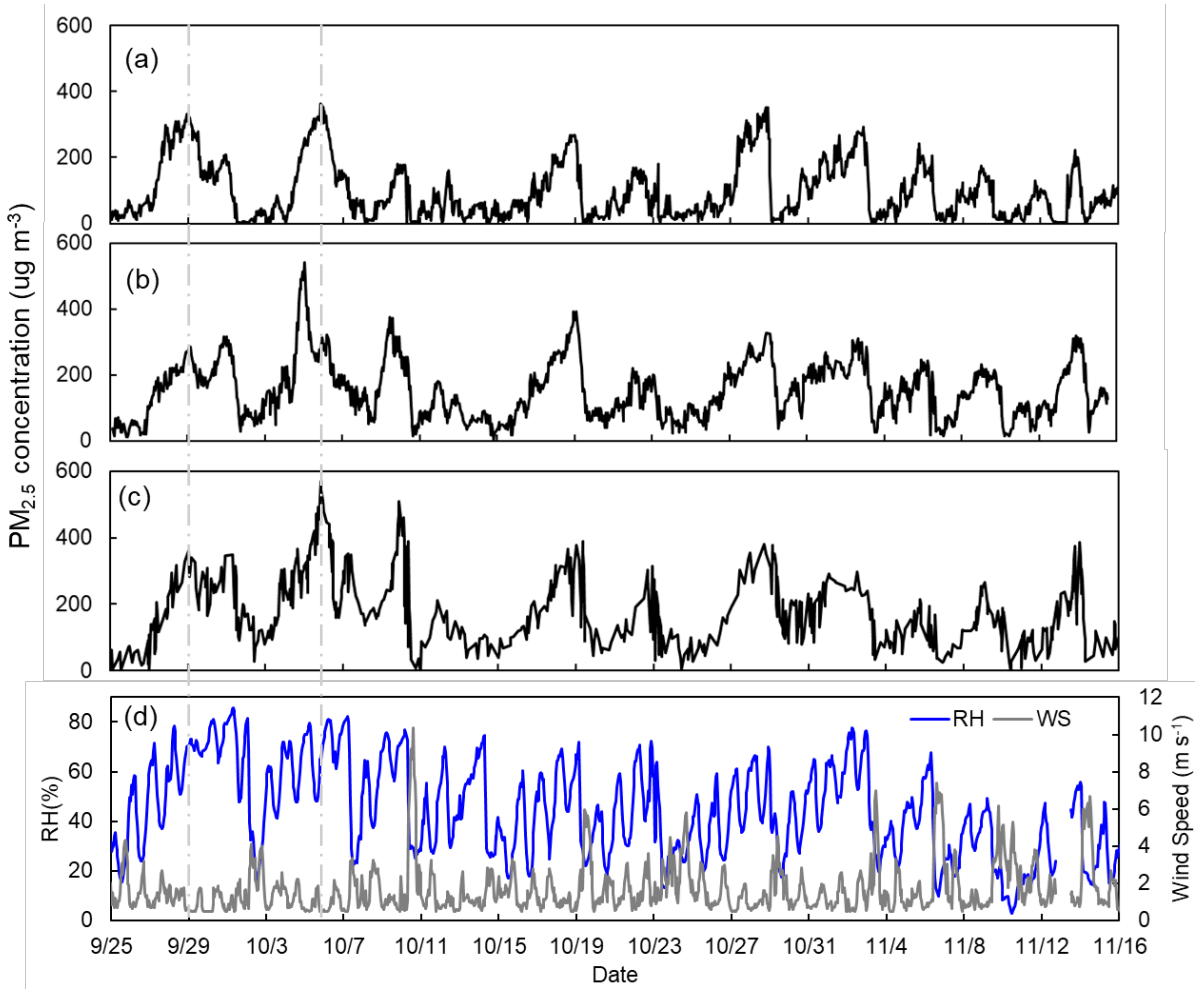

Figure 1. Time series of $PM_{2.5}$ mass concentration measured at three megacities over North China Plain (NCP), including (a) Beijing, (b) Baoding, and (c) Shijiazhuang from 25 September to 16 November, 2013, and (d) the associated relative humidity (RH, blue line) and 10-m wind speed (grey line) in Beijing. The $PM_{2.5}$ mass concentration and meteorological fields in Beijing are taken from Guo et al. (2014), and the $PM_{2.5}$ data for Baoding and Shijiazhuang are taken from https://air.cnemc.cn:18007/. Two severe haze episodes from 25-29 September and from 2-7 October are selected as the case studies in this work, and the two vertical dash lines label the time for the peak $PM_{2.5}$ concentration in Beijing.

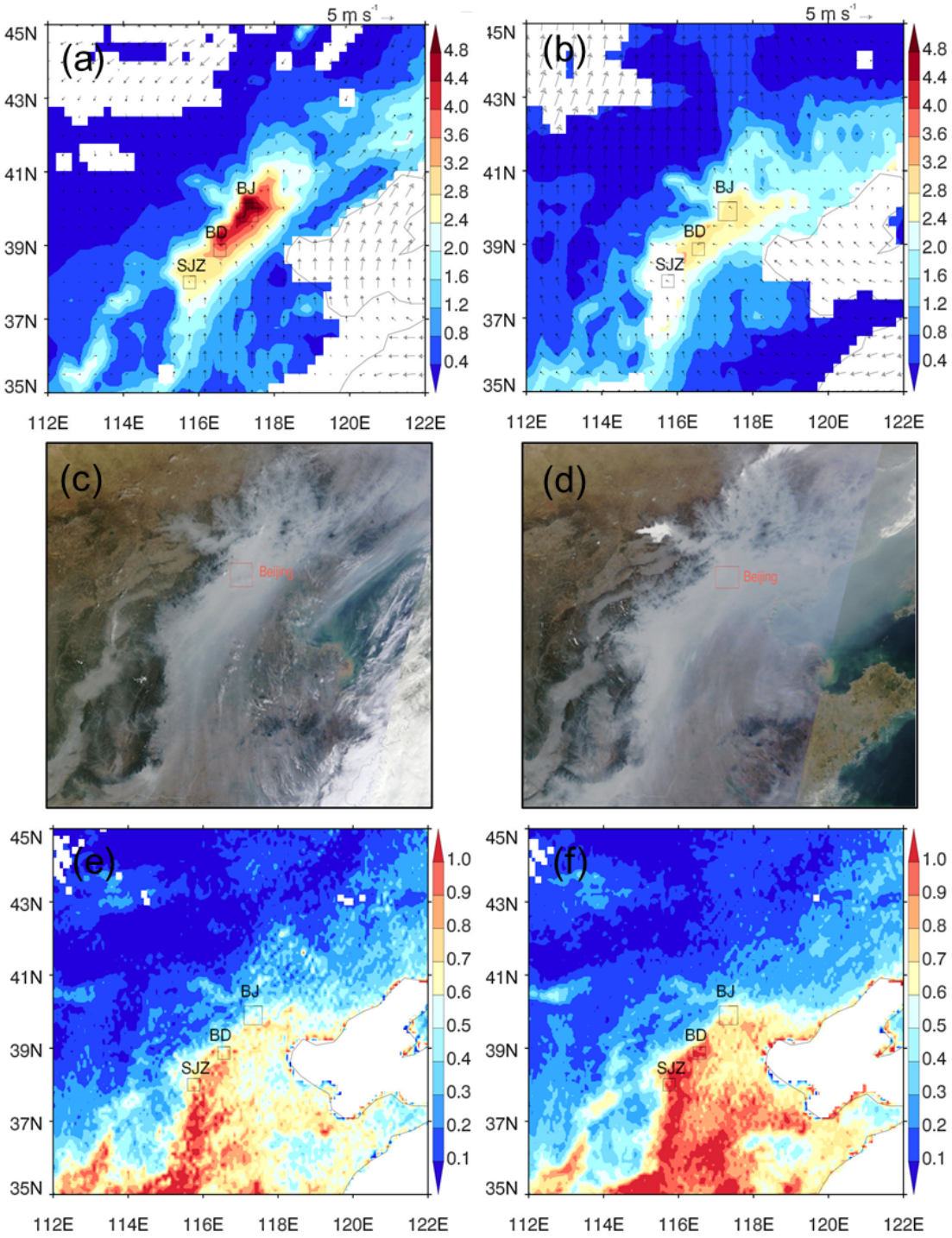

Figure 2. MODIS AOD (a-b) and visible images (c-d) illustrating the two severe haze episodes in Fig. 1. (a) and (c) correspond to 28 September, 2013, and (b) and (d) correspond to 5 October, 2013. (e) and (f) represent MODIS AOD of fall seasonal and annual mean in 2013. The megacities of Beijing (BJ), Baoding (BD) and Shijiazhuang (SJZ) are marked as squares. Wind field imposed on (a) and (b) is based on ECMWF reanalysis data.

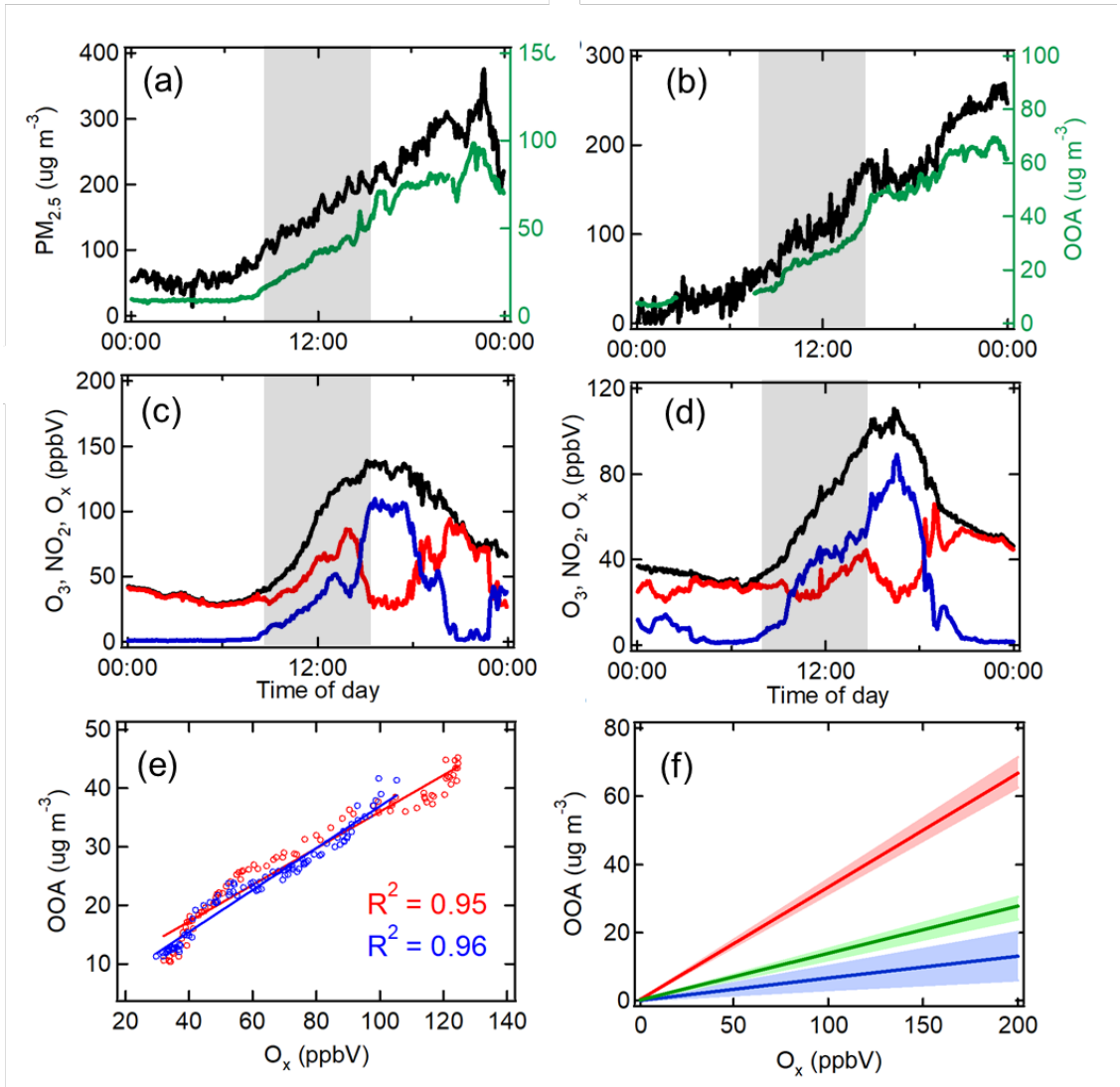

Figure 3. Temporal evolutions of measured $PM_{2.5}$ (black) and OOA (green) mass concentrations (a-b) and O_3 (blue), NO_2 (red), and O_x (black) mixing ratios (c-d) during the early stages of the two haze episodes. (a) and (c) are for the episode starting on 27 September, 2013, and (b) and (d) are for the episode starting on 4 October, 2013. (e) represents linear regression between O_x and OOA on 27 September (red circles) and 4 October (blue circles), 2013. The grey shadings (a-d) correspond to the largest variation in O_x, which covers both the clean and transition periods. (f) corresponds to the ratios of [OOA] changes to [O_x] changes (Δ[OOA]/Δ[O_x]) for Beijing (red), Mexico City (green) and Houston (blue). The ratios for Beijing are derived from this study, and the ratios for Mexico City and Houston taken from Wood et al. (2010). Color shadings in (f) represent the range between the minimum and maximum ratios.

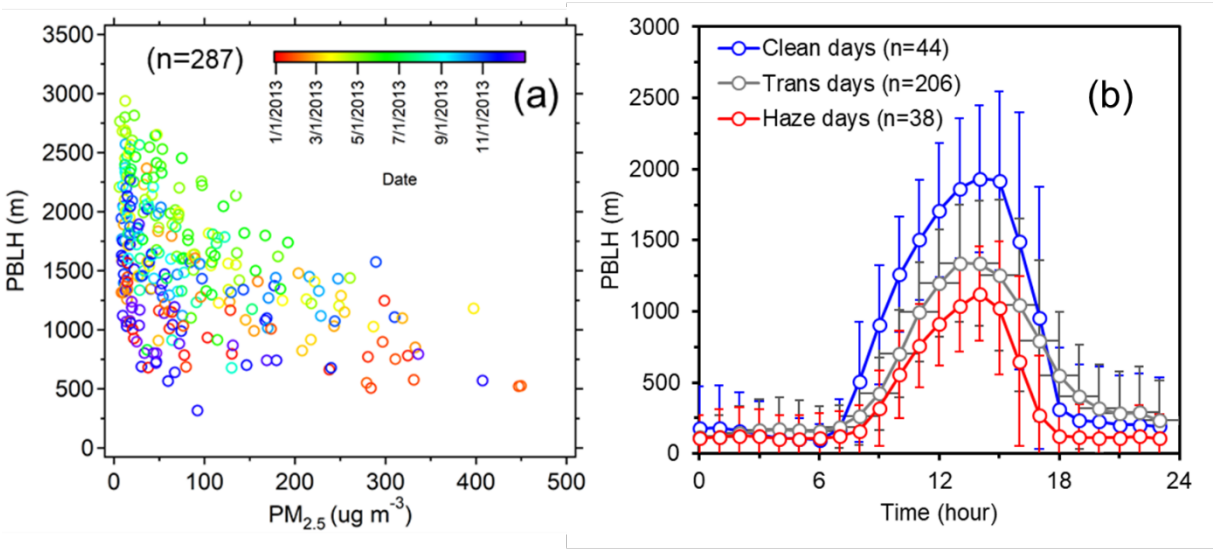

Figure 4. (a) Scattering plot for daily mean PBL height versus $PM_{2.5}$ concentration and (b) mean diurnal variations of PBL height averaged over clean days (daily mean $PM_{2.5} < 30$ μg m^{-3}), extremely hazy days (daily mean $PM_{2.5} > 200$ μg m^{-3}), and transition days (30 μg m^{-3} < daily mean $PM_{2.5} < 200$ μg m^{-3}) in 2013 at Beijing, China. *n* denotes the number of days used for plotting. The vertical lines in (b) denote ±1 standard deviation. All the precipitation days were filtered out.

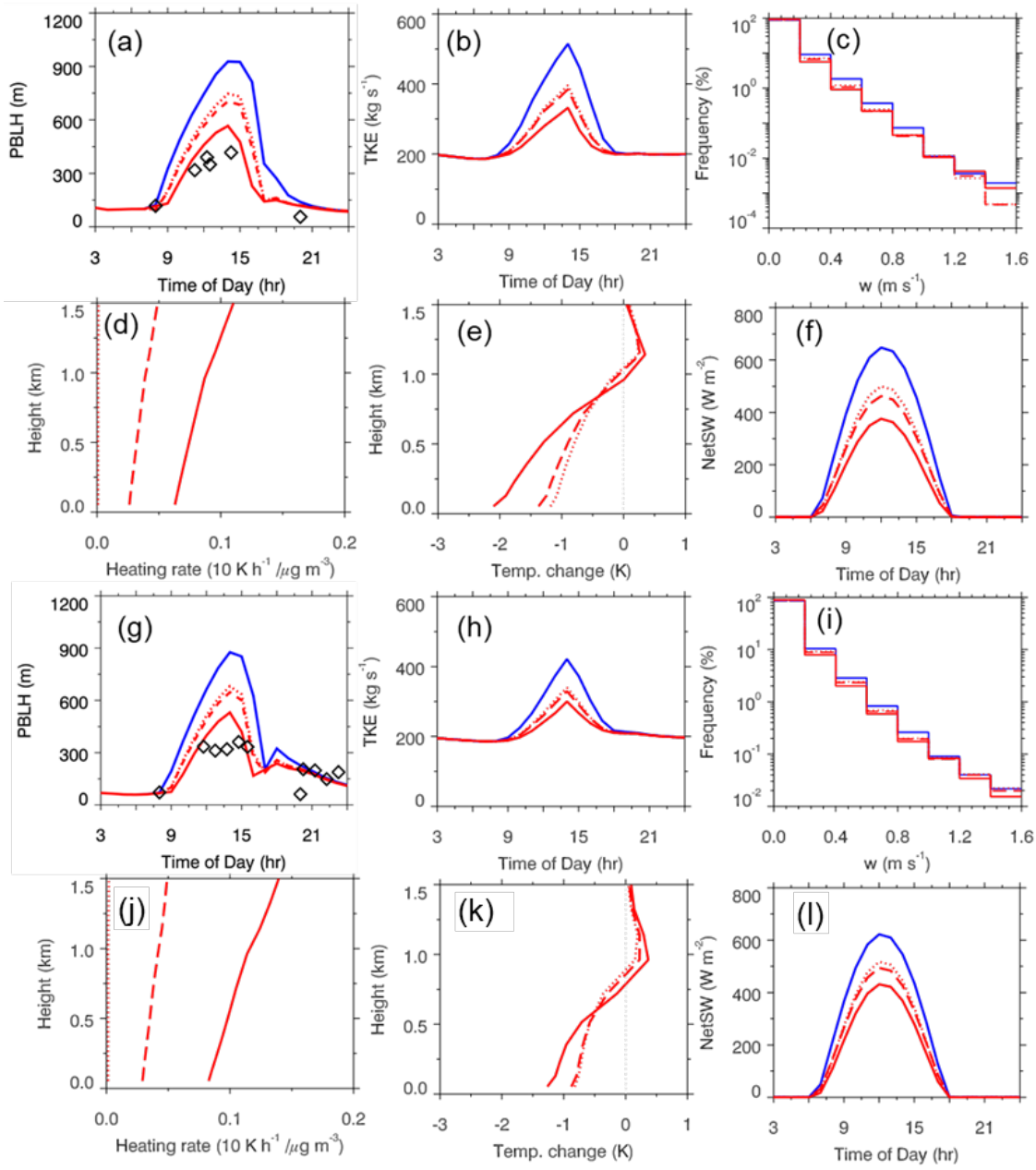

Figure 5. Simulated meteorological conditions and thermodynamic and dynamic feedbacks under the clean conditions (blue solid) and the polluted conditions for the non-BC (red dot), fresh-BC (red dashed), and aged-BC (red solid) cases. (a) and (g) correspond to simulated diurnal variations of PBL height, (b) and (h) correspond to the diurnal variations of vertically integrated TKE, (c) and (i) represent the frequency distribution of updraft. (d) and (j) are the vertical profile of the shortwave heating rate per unit aerosol mass for the non-BC (red dot line), fresh-BC (red dash line), and aged-BC (red solid line) cases. (e) and (k) are similar as (d) and (j) but for the temperature changes. (f) and (l) are diurnal evolutions of net surface shortwave radiation (NetSW). (a-f) are for EP1 and (g-n) are for EP2. The black hollow squares in (a) and (g) denote measurements of PBL height from ceilometer.

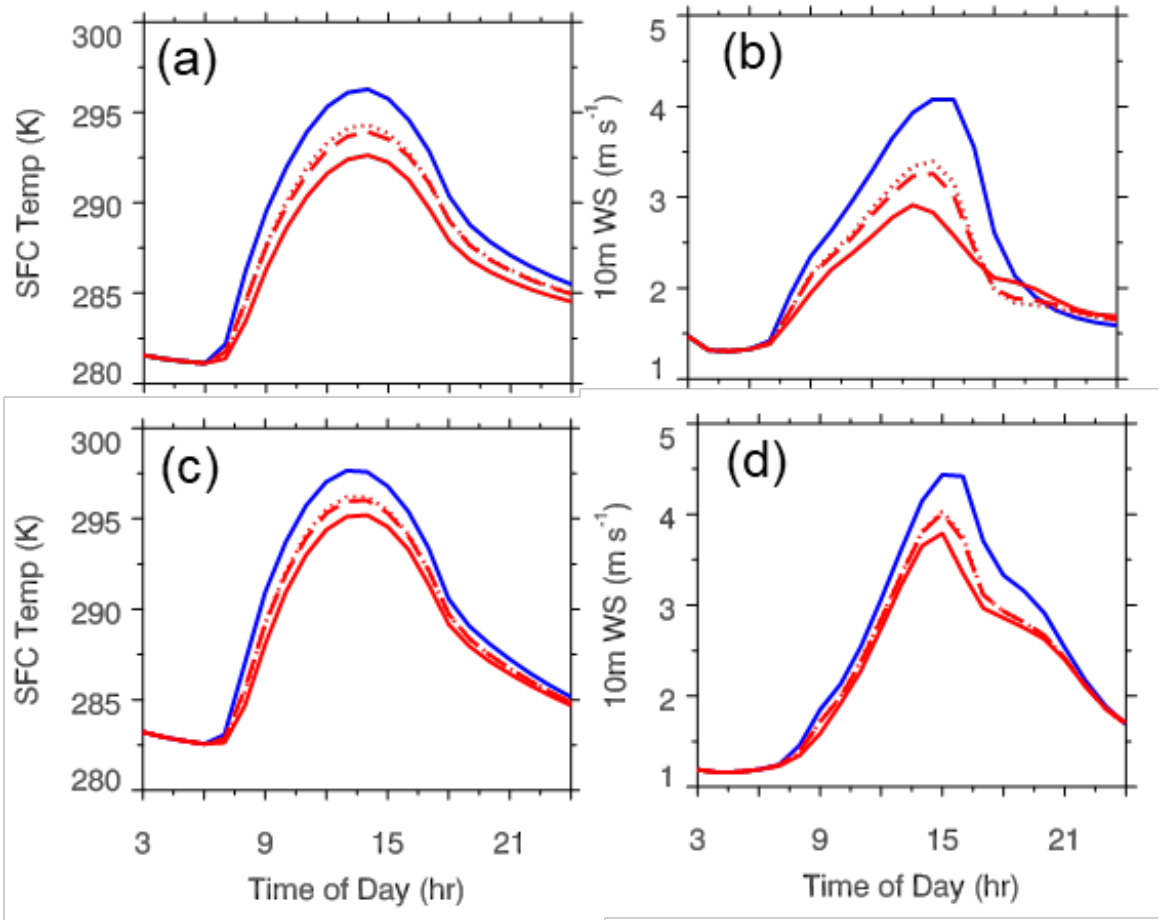

962
963 **Figure 6.** Temporal evolutions of surface temperatures (a and c) and 10-meter wind speeds (b
964 and d) under the clean conditions (blue solid) and the polluted conditions for the non-BC (red
965 dot), fresh-BC (red dashed), and aged-BC (red solid) cases. (a) and (b) correspond to EP1,
966 and (c) and (d) correspond to EP2.
967

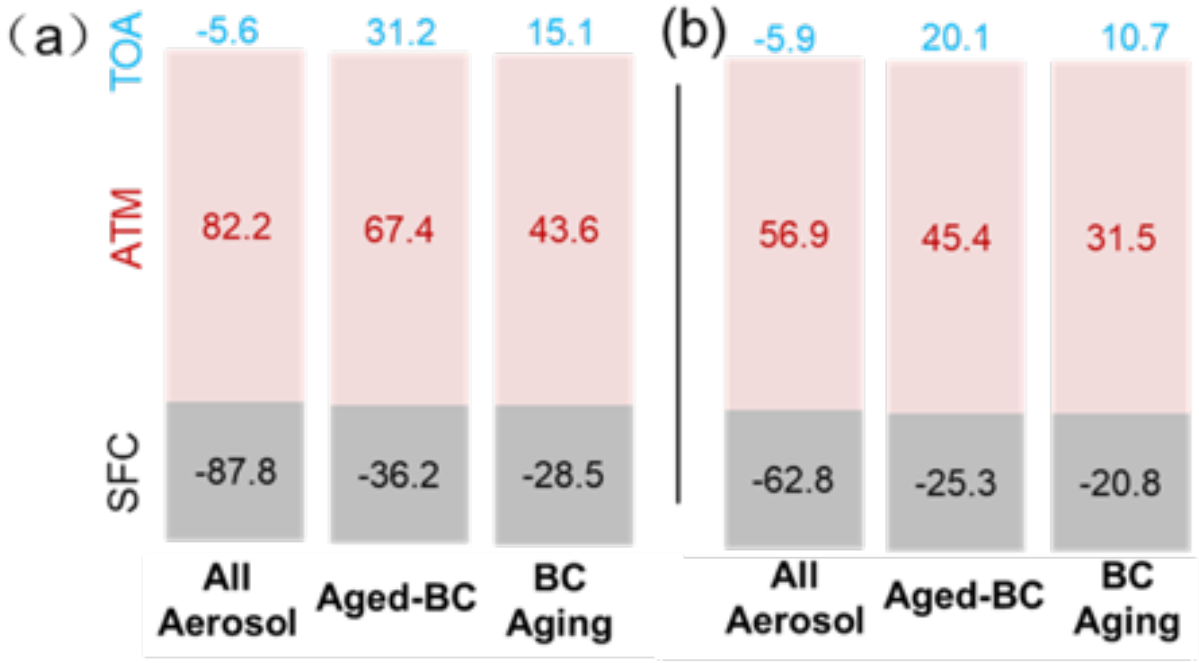

968

969 **Figure 7.** Aerosol direct radiative forcing for total aerosol (left column), aged-BC (middle
970 column), and BC aging (right column) on the top of the atmosphere (TOA), in the atmosphere
971 (ATM), and at the surface (SFC) for two severe haze days in Beijing. (a) and (b) correspond to
972 EP1 and EP2, respectively. The forcing caused by BC aging corresponds to the difference in
973 the simulations between the fresh-BC and aged-BC cases. The number denotes radiative
974 forcing in the unit of W m^{-2}.
975

976 **Table 1.** List of numerical experiments.
977

Case	Description
clean	Simulations with aerosol conditions from the days just before the two selected haze episodes start (25 September and 2 October 2013), with daily mean $PM_{2.5}$ < 30 μg m^{-3}.
aged-BC	Simulations on the most polluted days during the two haze episodes (28 September and 5 October 2013), with daily mean $PM_{2.5}$ > 200 μg m^{-3}. The core-shell configuration is assumed for BC and non-BC component mixing. The BC core is assumed as a sphere.
non-BC	The polluted cases but without BC radiative effects by turning off calculations of BC absorption and scattering.
fresh-BC	The polluted cases with fresh BC, in which the BC core is assumed as a sphere but not imbedded in the non-BC shell. The optical properties of the BC core are calculated externally using a Mie theory code. The lensing effect due to aging is not considered in this case.

978

Table 2. Comparisons between measurements and simulations for aerosol optical properties and surface solar radiation during the two haze episodes (EP1/EP2).

Case	SSA	AOD	Max solar radiation flux at surface (W m^{-2})	Accumulated surface solar radiation (MJ m^{-2})
E_{MAC-BC} = 2.4	0.83/0.83	3.7/2.1	342/403	10.1/11.5
Aged-BC	0.87/0.87	3.6/2.0	326/402	9.2/11.3
Observations	0.90[a]	3.5/2.4[b]	480[c]/452	10.6[c]/9.8

[a]SSA is based on a recent field campaign conducted in 2015 at Beijing.

[b]AOD is based on AERONET measurements at the Beijing site. (http://aeronet.gsfc.nasa.gov/).

[c]The maximum solar radiation flux and accumulated surface solar radiation were measured at China Meteorological Research Institute, Beijing, China.

Table 3. RH sensitivity to PBL height changes calculated using the empirical equations by Tie et al. (2017). PBL heights are from ceilometer measurements.

	Condition	Mixing Layer Height (meters)	RH	difference in RH (Clean - Hazy)
EP1	Hazy	395	68%	39%
	Clean	1180	29%	
EP2	Hazy	370	73%	45%
	Clean	1313	28%	